ORIGINAL ARTICLE

*Journal of Cachexia, Sarcopenia and Muscle* 2021; **12**: 1312–1332
Published online 6 July 2021 in Wiley Online Library (wileyonlinelibrary.com) **DOI:** 10.1002/jcsm.12745

# Physiologic and molecular characterization of a novel murine model of metastatic head and neck cancer cachexia

Brennan Olson[1,2], Mason A. Norgard[1], Peter R. Levasseur[1], Xinxia Zhu[1] & Daniel L. Marks[1,3,4]*

[1]*Papé Family Pediatric Research Institute, Oregon Health & Science University, Portland, OR, USA;* [2]*Medical Scientist Training Program, Oregon Health & Science University, Portland, OR, USA;* [3]*Brenden-Colson Center for Pancreatic Care, Oregon Health and & Science University Portland, OR, USA;* [4]*Knight Cancer Institute, Oregon Health & Science University, Portland, OR, USA*

## Abstract

**Background** Cancer cachexia is a metabolic disorder characterized by the progressive loss of fat and lean mass that results in significant wasting, ultimately leading to reduced quality of life and increased mortality. Effective therapies for cachexia are lacking, potentially owing to the mismatch in clinically relevant models of cachexia. Specifically, cachexia observed in a clinical setting is commonly associated with advanced or late-stage cancers that are metastatic, yet pre-clinical metastatic models of cachexia are limited. Furthermore, the prevalence of cachexia in head and neck cancer patients is high, yet few pre-clinical models of head and neck cancer cachexia exist. In addition to these shortcomings, cachexia is also heterogeneous among any given cancer, whereas patients with similar disease burden may experience significantly different degrees of cachexia symptoms. In order to address these issues, we characterize a metastatic model of human papilloma virus (HPV) positive head and neck squamous cell carcinoma that recapitulates the cardinal clinical and molecular features of cancer cachexia.

**Methods** Male and female C57BL/6 mice were implanted subcutaneously with oropharyngeal squamous cell carcinoma cells stably transformed with HPV16 E6 and E7 together with hRas and luciferase (mEERL) that metastasizes to the lungs (MLM). We then robustly characterize the physiologic, behavioural, and molecular signatures during tumour development in two MLM subclones.

**Results** Mice injected with MLM tumour cells rapidly developed primary tumours and eventual metastatic lesions to the lungs. MLM3, but not MLM5, engrafted mice progressively lost fat and lean mass during tumour development despite the absence of anorexia ($P < 0.05$). Behaviourally, MLM3-implanted mice displayed decreased locomotor behaviours and impaired nest building ($P < 0.05$). Muscle catabolism programmes associated with cachexia, including E3 ubiquitin ligase and autophagy up-regulation, along with progressive adipose wasting and accompanying browning gene signatures, were observed. Tumour progression also corresponded with hypothalamic and peripheral organ inflammation, as well as an elevation in neutrophil-to-lymphocyte ratio ($P < 0.05$). Finally, we characterize the fat and lean mass sparing effects of voluntary wheel running on MLM3 cachexia ($P < 0.05$).

**Conclusions** This syngeneic MLM3 allograft model of metastatic cancer cachexia is reliable, consistent, and readily recapitulates key clinical and molecular features and heterogeneity of cancer cachexia. Because few metastatic models of cachexia exist—even though cachexia often accompanies metastatic progression—we believe this model more accurately captures cancer cachexia observed in a clinical setting and thus is well suited for future mechanistic studies and pre-clinical therapy development for this crippling metabolic disorder.

**Keywords** Cachexia; Head and neck cancer; Metastasis; Inflammation; Muscle wasting; Fat wasting

*Received: 17 March 2021; Revised: 19 May 2021; Accepted: 8 June 2021*
**Correspondence to: Daniel L. Marks, Knight Cancer Institute, Oregon Health & Science University, 3181 SW Sam Jackson Park Road, L 481, Portland, OR 97239, USA. Email: marksd@ohsu.edu*

## Introduction

Cancer-associated cachexia is a metabolic disorder characterized by a progressive loss of body mass with preferential catabolism of muscle and adipose tissue.[1–3] In addition to physical deterioration, cachexia manifests distinct behavioural adaptations, including anorexia, fatigue, anhedonia, and cognitive decline.[1,4] These signs and symptoms of cachexia significantly influence patients' quality of life, ability to tolerate treatment, and eventual mortality.[5,6] Despite the prevalence and clinical burden cancer cachexia imposes, effective therapies are lacking. In fact, over 100 clinical trials of human cancer cachexia have been conducted to date, yet none resulted in the approval of an effective therapy.[7–11] This lack of translation from pre-clinical models of cachexia to human trials is not lost on those in the field of cachexia research, as there is a recent push to improve the predictive capacity of our commonly used rodent models of cachexia.[12] Specifically, researchers are suggesting using older animals, mimicking clinical treatment modalities, and models of recurrent and/or metastatic disease.[2,7,11,13–15] The latter is a particularly noticeable feature lacking from current animal models, as metastatic disease and cachexia are closely associated in a clinical setting,[16–19] and recent research suggests the metastatic cascade mediates unique systemic features of cachexia that cannot be solely explained by the biology of the primary tumour.[20–22]

To this end, we sought to establish and characterize a model of cancer cachexia that is technically simple, reliable, reproducible, and addresses several of the aforementioned concerns of current cancer cachexia models posed by researchers in the field. Specifically, we characterize a metastatic human papilloma virus (HPV) + squamous cell carcinoma model of head and neck cancer (HNC) cachexia that utilizes a metastatic cell line isolated from the lung from an animal that previously failed a cisplatin/radiation regimen.[23] Because it is estimated that cachexia affects nearly half of patients diagnosed HNC,[2,24–26] and very few HNC or recurrent/metastatic animal models of cachexia exist, we believe this model helps bridge this important gap in cachexia research.

Herein, we robustly characterize the molecular and behavioural features of mice injected with a syngeneic oropharyngeal squamous cell carcinoma cell line stably transformed with HPV16 E6 and E7 together with hRas and luciferase (mEERL) that metastasizes to the lungs (MLM).[23] Utilizing two MLM subclones with near-identical tumour growth trajectories, we observed heterogeneous cachexia responses to these two cell lines. Implantation of the MLM3 subclone resulted in significant muscle, fat, and body mass loss compared with the MLM5 subclone. Because MLM3-engraftment resulted in a significant wasting phenotype consistent with cachexia, we further characterized the behavioural and molecular features of MLM3 cachexia. Specifically, mice were assessed for gross fluctuations in body composition, including fat and lean mass atrophy, as well as commonly observed cachexia behaviours, including food intake and locomotor activities. Finally, we assess end-organ molecular adaptations associated with cancer-cachexia progression, including fast-twitch and slow-twitch fibre-enriched skeletal muscle groups, the central nervous system (CNS), heart, liver, spleen, brown (BAT) and white adipose tissue (WAT), as well as the blood/plasma.

## Methods

### *Mice*

Male and female C57BL/6 J mice were purchased from The Jackson Laboratory (WT, JAX catalogue number #000664) and maintained in our animal facility. All mice were housed and bred in a dedicated mouse room with a temperature 26°C with a 12 h light/dark cycle. Animals were provided *ad libitum* access to food and water (Purina rodent diet 5001; Purina Mills, St. Louis, MO, USA). For behavioural studies, animals were individually housed for acclimation for 7 days prior to tumour implantation. Tumour-bearing animals were euthanized according to the end points of tumour study policy. All mouse studies were conducted in accordance with the National Institutes of Health Guide for the Care and Use of Laboratory animals and approved by the Institutional Animal Care and Use Committee of Oregon Health & Science University.

### *Human papilloma virus + squamous cell carcinoma cell line and culturing*

The models of HPV + squamous cell carcinoma cachexia utilized herein are clonogenic cell lines derived from metastatic lung lesions from in a separate C57BL/6 J mice implanted with a parental HPV + squamous cell carcinoma [expressing HPV16 E6/E7, hRas, and luciferase (mEERL)] subcutaneously that failed cisplatin/radiation therapy.[23] In this study, we perform cachexia analysis on four mEERL lung metastasis (MLM1, MLM3, MLM5, & MLM10) described by Vermeer *et al*. and observe MLM3 as the only metastatic cell line associated with significant lean and fat mass loss (data not shown), thus we

focus our subsequent analysis on this cell line.[23] All cell lines were maintained in DMEM supplemented with 10% foetal bovine serum, 1% minimum essential medium non-essential amino acids, 1 mM sodium pyruvate, and 50 U/mL penicillin/streptomycin (Gibco), in cell incubators maintained at 37°C and 5% $CO_2$. All cell lines were routinely tested and confirmed negative for mycoplasma contamination.

## *Generation of head and neck cancer model*

C57BL/6 mice aged 10–12 weeks were inoculated subcutaneously with an inoculum of $3 \times 10^6$ MLM tumour cells, while controls received heat-killed cells in the same volume. Subcutaneous implantation was performed in the right hind flank with a 300 μL injection of cell suspension in DMEM under isoflurane anaesthesia. Tumour growth was measured as previously described.[27]

## *Analysis of cachexia*

Food intake (with daily collection of spilled food mass with a bedding sieve), body mass, and post-procedure health status were monitored daily. Body temperature and voluntary locomotor activity (LMA) were measured via implanted MiniMitter tracking devices on 5 min recording intervals (MiniMitter, Bend, OR, USA). Voluntary wheel running was measured continuously utilizing lab-constructed wheels with digital revolutions counter. Necropsy tissue analysis included tumour, gastrocnemius, soleus, tibialis anterior, quadriceps, and heart mass by observers blinded to treatment groups. Additionally, hypothalamus, heart, gastrocnemius, soleus, tibialis anterior, quadriceps, and liver tissues were immediately flash frozen for gene expression analysis.

## *Nuclear magnetic resonance imaging*

Nuclear magnetic resonance (NMR) measurements were taken at the beginning of designated studies with concurrent balancing of weight and body composition measures between sham and tumour groups. For repeated measures studies, body composition was assessed at the designated time points, while terminal body composition was performed on animal carcasses after primary tumour excision.

## *Immunohistochemistry*

At the end of a study, mice were deeply anaesthetised using a ketamine/xylazine/acepromazine cocktail and sacrificed by transcardial perfusion with 20 mL PBS followed by ice cold 4% paraformaldehyde. Tissues were post-fixed in 4% paraformaldehyde overnight at 4°C prior to sectioning protocols.

### Brain samples

After post-fixation, brains were cryoprotected in 20% sucrose for 24 h at 4°C prior to 30 μM microtome sectioning. Free-floating sections were incubated in blocking solution (5% normal donkey serum in 0.01 M PBS and 0.3% Triton X-100) for 30 min at room temperature, followed by primary antibody incubation (listed below) overnight at 4°C. Sections were thoroughly washed with PBS between steps. Sections were mounted on gelatine-coated slides and coverslipped with Prolong Gold anti-fade media with DAPI (Thermofisher).

Fluorescent-based images of the hypothalamus were acquired on a Nikon confocal microscope. Primary antibodies utilized above are listed with company, clone, host, species, and concentration defined in parentheses, respectively: mouse anti-GFAP (Millipore, GA5, 1:1000) and rabbit anti-Iba-1 (Wako, NCNP24, 1:1000). The following secondary antibodies were used, all derived from donkey: anti-mouse AF488 (1:500) and anti-rabbit AF555 (1:1000).

## *Enzyme-linked immunosorbent assay*

Whole blood was harvested from mice by cardiopuncture, and plasma was isolated using $K_2$EDTA tubes (BD 365974). Mouse plasma parathyroid hormone-related protein (PTHrP) concentrations were assayed by ELISA according to the manufacturer's protocol (LSBio, Catalogue #LS-F15276).

## *Quantitative real time PCR*

Snap-frozen tissues were rapidly homogenized and RNA was purified with an RNeasy Mini Kit (Qiagen). Samples were then reverse-transcribed with the High Capacity cDNA Reverse Transcription Kit (Life Technologies). Quantitative real time PCR was performed using TaqMan primer probes. Tissues were normalized to 18S using the ddCT method for analysis.

## *Clinical assays*

Adaptive and innate immune cell counts were performed on EDTA-decoagulated plasma samples using HemaVet 950 (Drew Scientific). Blood glucose was measured immediately prior to euthanasia with electronic glucometer (OneTouch Ultra).

## *Statistics*

All statistical analyses for murine data were performed in GraphPad Prism 8.0 software. Quantitative data are reported as mean ± standard error. For comparison between tumour and control groups, data were assessed by Student's *t*-test, one-way ANOVA, or two-way ANOVA if sex was a variable.

For all analyses, a $P$ value of $<0.05$ was considered to be statistically significant. All measurements were from distinct samples and not taken from the same sample more than once.

# Results

## *The MLM3 clone is particularly cachexigenic*

Because cachexia is broadly heterogeneous and influenced by several host and tumour parameters, we first sought to determine if the equivalently growing MLM3 and MLM5 subclones induced a similar degree of cachexia-associated wasting.[23] Consistent with studies performed by Vermeer *et al*., the MLM3 and MLM5 clones display equivalent primary tumour growth in our studies (*Figure* 1A; Supporting Information, *Figure* S1A).[23] However, despite this nearly identical primary tumour growth, MLM5 implantation resulted in a modest loss of body mass compared with sham controls, while MLM3-implanted mice displayed a progressive loss of body mass (*Figure* 1B). Tumour-free body mass at the study's end were consistent with these repeated body mass measures, demonstrating lessened tumour-free body mass loss in MLM5-engrafted mice compared with MLM3-engrafted mice (*Figure* 1C). We observed no differences in food consumption for MLM3-engrafted male mice compared with sham controls, yet MLM5-engrafted male mice demonstrated a modest hyperphagia phenotype (*Figure* 1D). Consistent with the progressive loss of body mass, MLM3-engrafted mice display a significantly increased fat wasting phenotype compared with MLM5-engrafted mice (*Figure* 1E–1F). Additionally, whole-body lean mass, terminal gastrocnemius mass, and terminal cardiac tissue mass were significantly decreased in the MLM3-engrafted mice when compared with both sham and MLM5-engrafted mice (*Figure* 1G–1I). The improvement in gross skeletal muscle mass in MLM5-engrafted mice was associated with decreased ubiquitin ligase expression in the gastrocnemius muscle (*Figure* S1B). MLM5 mice displayed significantly increased blood glucose levels at the time of sacrifice compared to MLM3-engrafted mice, potentially owing to their improved caloric intake (*Figure* S1C).[28] MLM5-engrafted mice displayed an intermediate hepatic inflammatory gene profile between sham and MLM5-engrafted mice, as indicated by *Il-1β*, *Il-6*, and *Orm1* gene expression, although none of these were significantly altered compared with the MLM3 group alone (*Figure* S1D). Interestingly, MLM5-engrafted mice displayed significantly larger spleens compared with the MLM3 group (*Figure* S1E). Taken together, MLM3 and MLM5 cell lines display similar growth *in vivo*, yet demonstrate drastically different wasting phenotypes. These studies serve not only to validate the utility of MLM3 as a unique model of cancer cachexia but also to provide an invaluable comparator in MLM5 due to its significantly reduced cachexia phenotype. Future *in vivo* and *in vitro* studies comparing these two tumour models could prove useful for the identification of tumour-specific cachexia 'factors' that may drive wasting in MLM3, but not MLM5.

## *MLM3 implantation results in the clinical signs and symptoms of cachexia in both male and female mice*

With the identification of significant lean and fat mass catabolism in MLM3-engrafted male mice, we sought to further characterize the wasting features of MLM3 in both male and female mice. Indeed, subcutaneous implantation of MLM3 cells result in sickness behaviours associated with cachexia in both male and female models, including the progressive loss of body mass over the course of tumour development (*Figure*s 2A and S2A–S2C). Consistent with Vermeer *et al*.'s observations, MLM3-engrafted male mice consistently display metastatic lesions in the lung, while we observed variable degrees of lung metastases in female MLM3-engrafted mice (*Figure* S2D–S2E). Metastases in other organs besides the lungs were not observed. Both male and female MLM3-implanted mice displayed a significant loss of body mass at the necropsy as indicated by tumour-free mass (*Figure* 2B). When monitoring food daily food intake, male mice exhibited no alterations in food consumption between tumour and sham groups, while female tumour-bearing mice experienced a phase of relative hyperphagia starting at Day 13 after tumour implantation (*Figure* 2C). Because cachexia is associated with preferential catabolism of fat and lean mass, we assessed both fat and lean compartments by NMR imaging. MLM3-engrafted males exhibited a progressive reduction in total-body fat mass, whereas tumour-bearing female mice lost a significant portion of their baseline fat mass early in the study (*Figure* 2D). Because portions of the tumour mass encode as lean mass by NMR, we assessed tumour-free lean mass at the study's end. Indeed, we observed a significant loss of total-body lean mass at the time of sacrifice in males, but not females (*Figure* 2E). Finally, we assessed sham and tumour-implanted mice's willingness to build nests at 7 day intervals throughout the study. Because nest building is an enjoyable activity for mice, but also an evolutionarily conserved behaviour to insulate animals and conserve energy during sleep, nest building is a useful surrogate measure of anhedonia and overall well-being.[29] Tumour-implanted mice displayed a significant reduction in nest-building behaviours at only advanced-stage disease (Day 21 post-implantation). Collectively, we conclude that the MLM3 implantation results in a progressive loss of body mass, preferential catabolism of fat and lean mass, as well as decreased overall health and well-being, measures consistent with cachexia observed in a clinical setting.

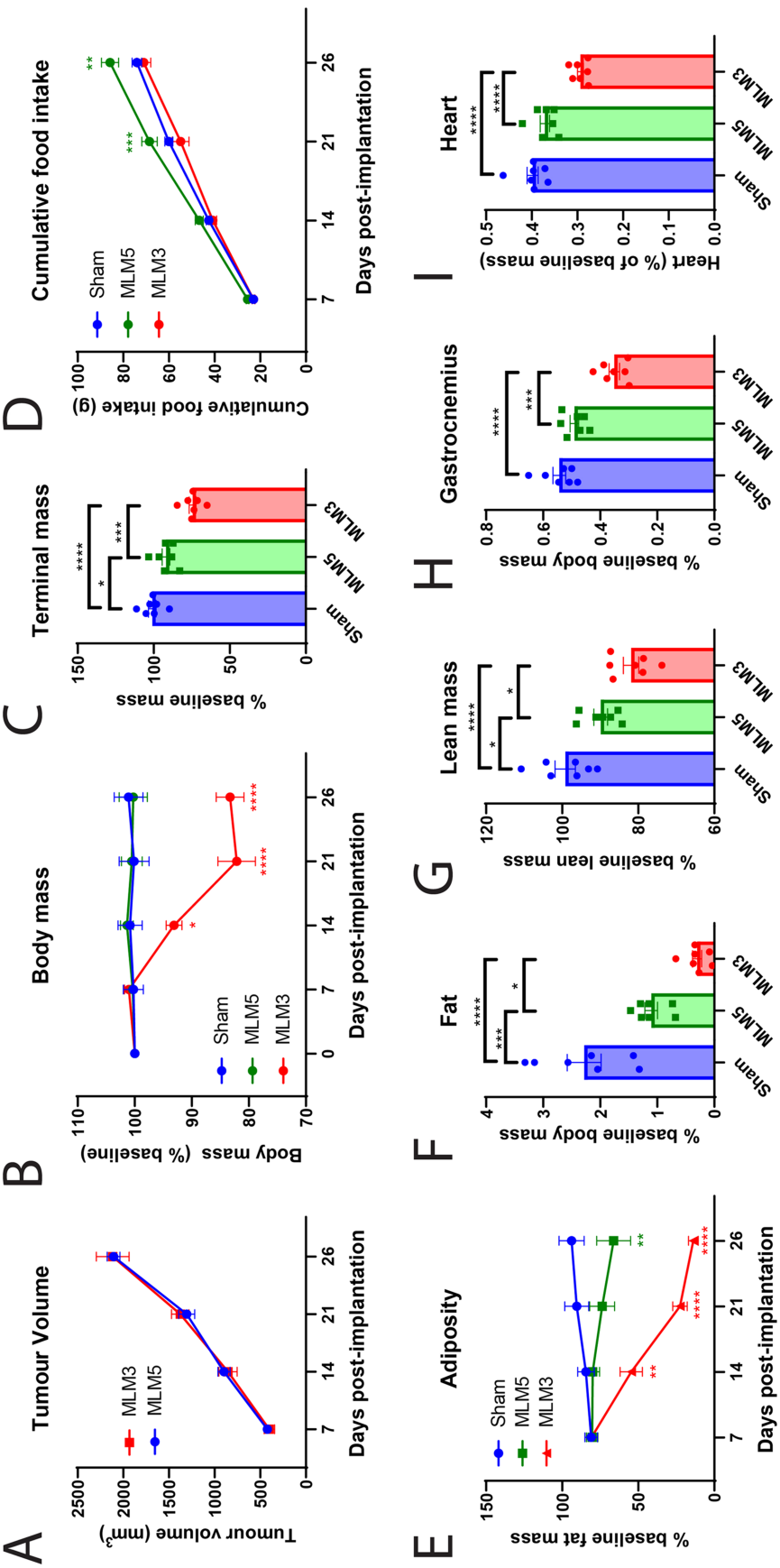


**Figure 1** MLM3 engraftment results in significantly increased muscle and fat catabolism compared with the MLM5 subclone. *(A)* Tumour volume in MLM3 and MLM5 engrafted male mice. *(B)* Sequential and *(C)* tumour-free body mass in sham, MLM3-implanted, and MLM5-implanted mice. *(D)* Cumulative food intake in sham, MLM3-implanted, and MLM5-implanted mice. *(E)* Sequential NMR fat mass and *(F)* terminal gonadal WAT mass. *(G)* Terminal lean mass NMR, *(H)* gastrocnemius mass, and *(I)* cardiac tissue mass. All data are expressed as mean ± SEM. $^{*}P \leq 0.05$, $^{**}P \leq 0.01$, and $^{***}P \leq 0.001$. $N = 7$ per group.

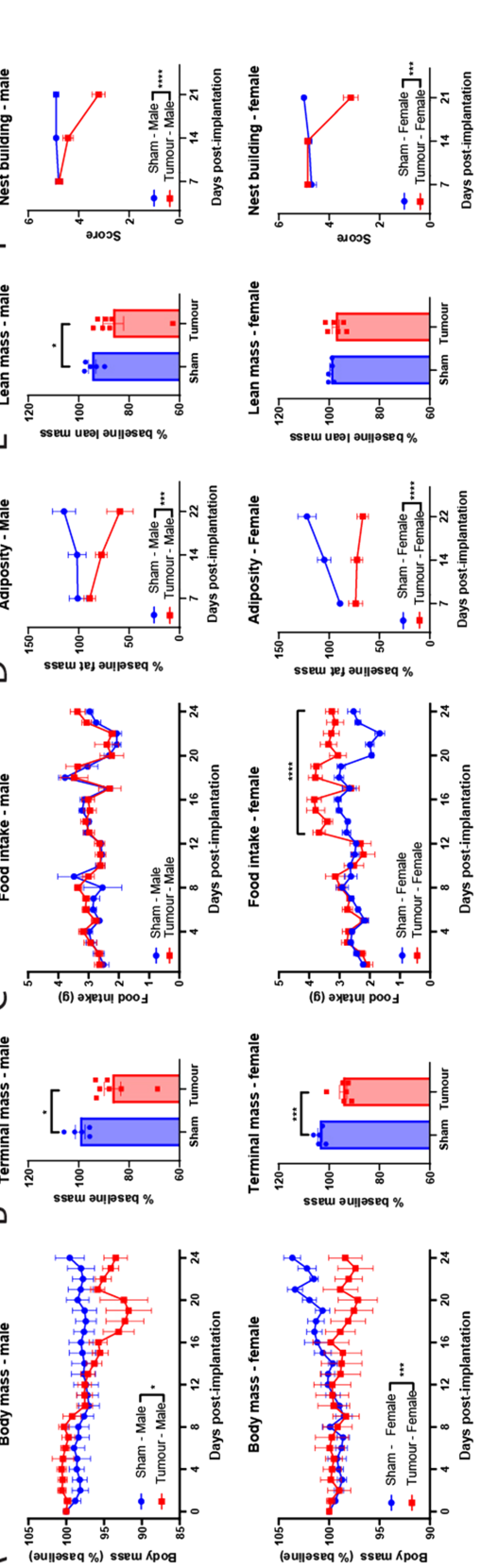


**Figure 2** MLM3 implantation recapitulates key clinical signs and symptoms of cachexia. *(A)* Daily and *(B)* tumour-free body mass in MLM-engrafted and sham-operation controls in male and female cohorts. *(C)* Daily food intake in MLM-engrafted and sham-operation controls in male and female cohorts. *(D)* Sequential NMR fat mass and *(E)* terminal lean mass measures. *(F)* Sequential nest-building scores. $N = 5–7$ per group. All data are expressed as mean ± SEM. $^{*}P \leq 0.05$, $^{**}P \leq 0.01$, and $^{***}P \leq 0.001$.

## *MLM3 engraftment results in progressive reduction in locomotor behaviours*

Because fatigue and lethargy produce significant impairments in patients' quality of life, future models of cancer cachexia should recapitulate these important clinical symptoms.[1,2] Thus, we sought to characterize home-cage LMA and voluntary wheel running throughout the course of MLM3 cachexia development in male mice. In assessing home-cage LMA, we divided activity into 12 h light and dark cycles that correspond with sleep and wake cycles and created tertile cachexia bins in accordance with the weight loss trajectory observed in *Figure* 2A (whereas minimal weight change is observed in the first third of the study). MLM3 tumour implantation resulted in a reduction of wake cycle activity beginning on Day 8 post-implantation (*Figure* 3A–3B), while sleep cycle activity was largely unaffected (*Figure* 3C–3D). We also assessed voluntary wheel running behaviours in MLM3 implanted mice, as this behaviour is not only a measure of tumour-associated fatigue but also hedonic activity, as non-captive mice will elect to run on a wheel for long periods without incentive.[30] Indeed, we observe a progressive reduction in wheel running in MLM3 implanted mice, with a significant and sustained reduction in wheel running starting Day 7 post-implantation (*Figure* 3E–3G). The consistent and progressive decline in both home-cage LMA and voluntary wheel running in this cachexia model demonstrates its utility in studying this important facet of cancer cachexia.

## *Lean mass catabolism associated with MLM3-cachexia is driven by autophagy and ubiquitin-ligase pathways*

Because cardinal features of clinical cachexia include progressive muscle and fat catabolism, pre-clinical models should recapitulate these wasting trajectories, both grossly and molecularly. Here, we characterized skeletal and cardiac tissue catabolism in MLM3-engrafted mice and observed significant lean mass wasting at the study's end. In the skeletal muscle compartment, MLM3-engrafted mice displayed significant wasting of fast-twitch fibre muscles, including the gastrocnemius, quadriceps, and tibialis anterior muscle (*Figure* 4A–4C). The soleus, a slow-twitch fibre muscle, also displayed significant catabolism (*Figure* 4D). Consistent with other pre-clinical models of cancer cachexia, including the $KRAS^{G12D}$ $P53^{R172H}$ Pdx-$Cre^{+/+}$ pancreatic ductal adenocarcinoma (KPC),[31] Lewis lung carcinoma (LLC),[32,33] and C26 colorectal adenocarcinoma (C26),[34] MLM3-engrafted mice display a significant induction of the E3 ubiquitin ligase genes *Mafbx*, *Murf1*, and *Foxo1* in skeletal muscle (*Figure* 4E). Cardiac tissue atrophy was measurable in male tumour-bearing mice, whereas females were resistant to cardiac wasting (*Figure* 4F). Despite minimal alterations in gross cardiac

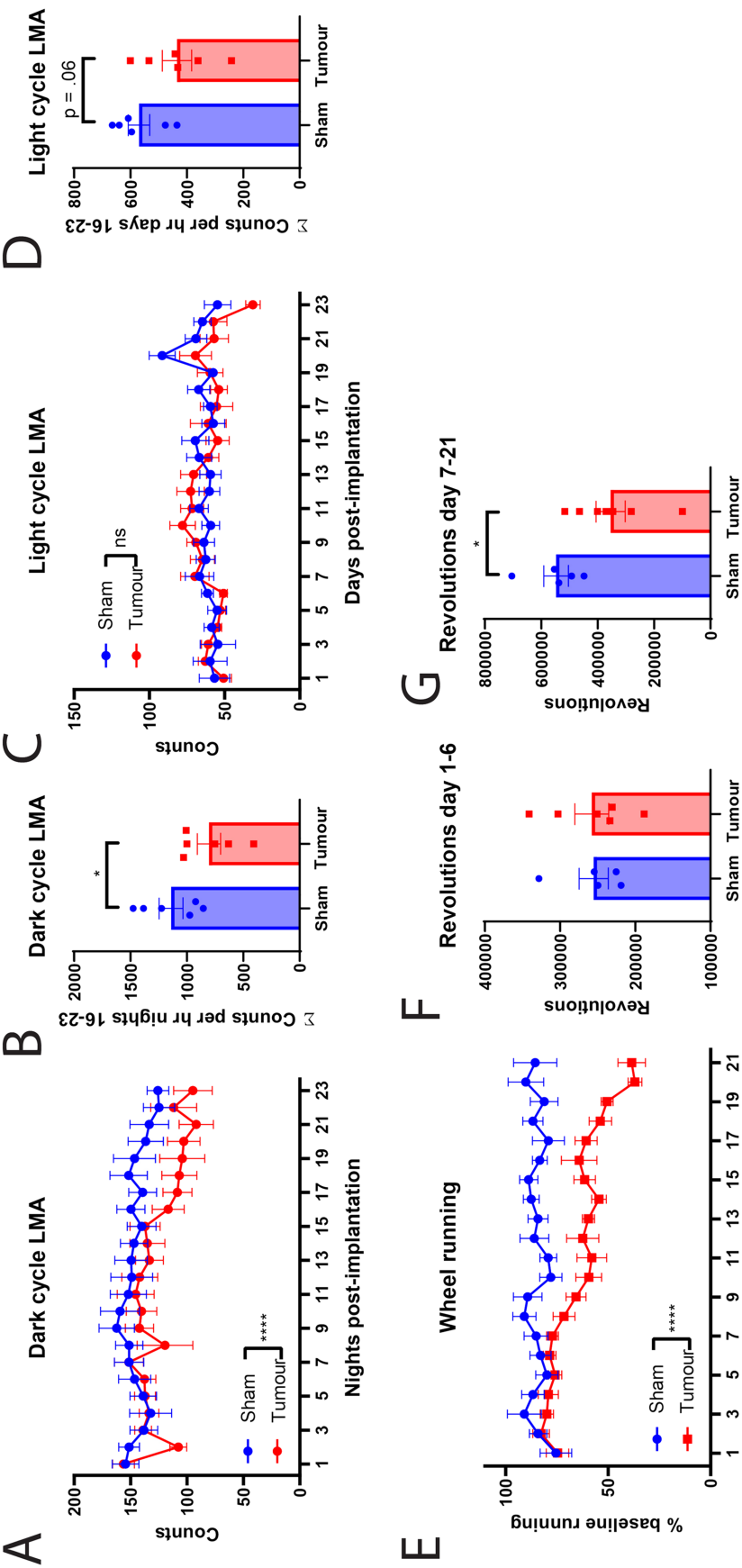


**Figure 3** MLM3 implantation results a progressive decline in home-cage locomotion and voluntary wheel running behaviours. *(A)* Daily dark cycle locomotor activity in counts per hour and *(B)* cumulative counts per hour from Days 16 to 23 (late cachexia). *(C)* Daily light cycle locomotor activity in counts per hour, and *(D)* cumulative counts per hour from Days 16 to 23 (late cachexia). *(E)* Daily voluntary wheel running as a percentage of baseline running. Cumulative revolutions from study Days *(F)* 1–6 and *(G)* 7–21. *(A–D)* $N = 6$ per group. *(E–G)* $N = 5$–6 per group. All mice were male. All data are expressed as mean ± SEM. $^{*}P \leq 0.05$, $^{**}P \leq 0.01$, and $^{***}P \leq 0.001$. LMA, locomotor activity.

wasting as indicated by organ mass, we observed a significant induction of autophagy genes *Cstl*, *Gabarapl*, and *Bnip3* in MLM3-engrafted mice (*Figure* 4G). While these autophagy-related genes were significantly regulated during MLM-cachexia in the heart, E3 ubiquitin ligase genes *Mafbx*, *Murf1*, and *Foxo1* were not significantly alerted in the heart between tumour and sham mice (*Figure* 4H). Collectively, the lean mass wasting observed in MLM3-engrafted mice is driven by activation of ubiquitin proteasome and autophagy pathways, two key catabolic pathways that drive cachexia-associated wasting in other highly studied murine models.

## *MLM3-cachexia results in fat mass wasting, browning of white adipose tissue, and elevation of core body temperature*

Another important facet of cancer cachexia that accompanies the progressive loss of fat mass is the metabolic reprogramming in this tissue that activates thermogenic pathways. In both pancreatic and lung cancer genetically engineered mouse models of cachexia, the browning of WAT corresponded with increased systemic energy expenditure.[35] In the present model of MLM3 cachexia, we observe significant wasting of WAT (*Figures* 5A and S3A) and elevation of browning genes *Ucp1* and *Cidea*, yet decreased expression of *Prdm16* and *Ppar-*$\gamma$ (*Figure* 5B). In comparing MLM3 and MLM5 models, although expression of *Ucp1* was lower in MLM5 relative to MLM3 mice, this difference was not significant. However, *Cidea* was significant down-regulated in MLM5 mice compared with MLM3 (MLM5:MLM3 RQ = 0.42, $p$ = 0.04). In BAT, we also observe a significant increase in thermogenesis gene *Ucp1* (*Figures* 5C and S3B), although these gene expression results are only associative when discussing thermogenic function of the resulting protein. The observed thermogenesis programmes induced in in the fat of MLM3-engrafted mice were independent of PTHrP, as neither male nor female cohorts exhibited an increase in circulating levels (*Figure* S3C–S3D). Because we observed an elevation in thermogenesis genes in both WAT and BAT, we next monitored core body temperature during the development of MLM3-cachexia. Tumour-bearing mice displayed an elevation in core body temperature during both light and dark cycles early-stage to mid-stage disease (Days 7–14), while temperatures approached that of control mice during late-stage cachexia (Days 15–22/23) (*Figure* 5D–5E).

## *MLM3-cachexia results in hypothalamic inflammation*

Because the hypothalamus is a critical CNS structure in regulating metabolic and behavioural programmes, and a growing body of evidence implicate aberrant hypothalamic processes in cachexia pathology, we sought to determine if MLM-cachexia is associated with hypothalamic inflammation as observed in other models of cancer cachexia.[31,36–38] We observe a robust elevation of inflammatory cytokine *Il-1*$\beta$, but no alterations in *Il-6*, *Nos2*, *and Tnf-*$\alpha$ (*Figure* 6A). In addition to an elevation of inflammatory cytokine expression in the mediobasal hypothalamus during cachexia, infiltration of peripheral immune cells was recently identified as a mediator of cachexia symptoms in the KPC pancreatic cancer model.[36] We observe a significant elevation of cell adhesion molecule *Selp*, chemokines *Cxcl1*, and chemokine-inducer and neutrophil chemoattractant *Lcn2*,[39,40] while *Cxcl10* is down-regulated, and *Cxcl2* and *Ccl2* were unaffected by tumour engraftment (*Figure* 6B). Interestingly, the orexigenic peptide *Agrp* was significantly elevated in both male and female tumour-bearing mice, although only MLM3-engrafted females exhibited hyperphagia at the time of sacrifice (*Figure* 6C). In addition to the transcriptional inflammatory profile observed in the hypothalamus of MLM3-engrafted mice, we observed an increase in microglia and astrocytes in the median eminence, a circumventricular organ that contains an attenuated blood–brain barrier (*Figure* 6D–6F). The arcuate nucleus and ventromedial hypothalamic nucleus demonstrated an increase in astrocytes in the MLM3 group but no difference in the number of microglia (*Figure* 6D–6F).

## *MLM engraftment results in neutrophil expansion and elevated neutrophil-to-lymphocyte ratio*

A burgeoning area of cachexia research describes how the immune system influences biological processes, including metabolism, inflammation, and neuroendocrine function.[36,37,41] Indeed, the emerging field of immunometabolism is now gaining traction in the field of cancer cachexia, as both immunologic and metabolic derangements contribute to the pathogenesis of cachexia. Thus, models of cachexia should recapitulate not only the behavioural and metabolic features of cancer progression but also the immunologic features of advanced disease. To this end, decades of research describe an elevation of neutrophil-to-lymphocyte ratio (NLR) as a negative prognostic factor in several cancer types, including HNCs,[42] and recent studies link elevated NLR to significant weight loss and cachexia.[43] MLM3 engraftment and subsequent development of cachexia results in a significant leukocytosis, which is largely driven by an absolute and relative increase in circulating neutrophils in both male and female models (*Figure* 7A–7E). At the time of sacrifice, both male and female engrafted mice display a large increase in NLR, with tumour-bearing females experiencing the highest ratio (*Figure* 7F). We also observed a significant decrease in mean corpuscular haemoglobin levels for both males and female mice, while mean platelet volume and total platelet

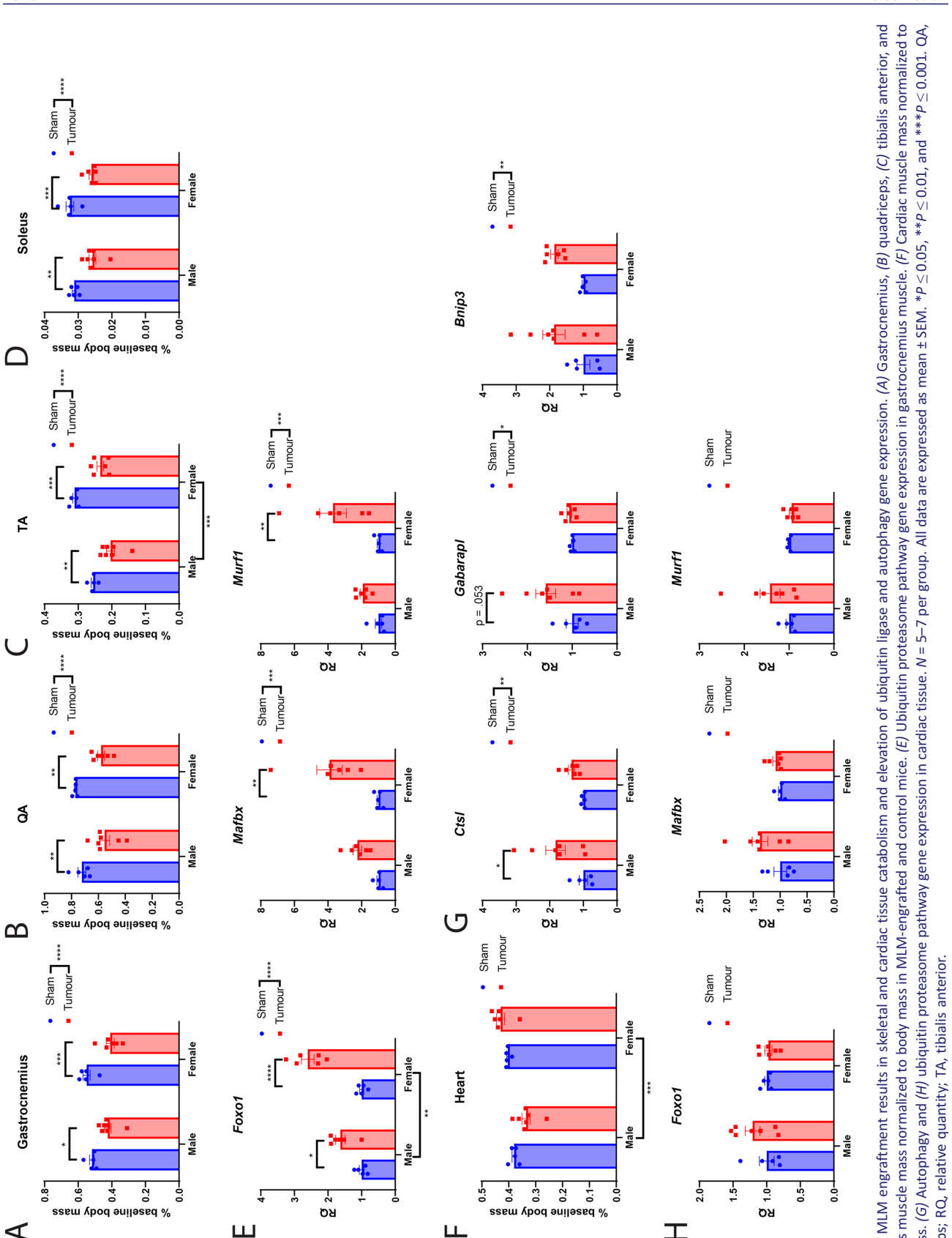


**Figure 4** MLM engraftment results in skeletal and cardiac tissue catabolism and elevation of ubiquitin ligase and autophagy gene expression. *(A)* Gastrocnemius, *(B)* quadriceps, *(C)* tibialis anterior, and *(D)* soleus muscle mass normalized to body mass in MLM-engrafted and control mice. *(E)* Ubiquitin proteasome pathway gene expression in gastrocnemius muscle. *(F)* Cardiac muscle mass normalized to body mass. *(G)* Autophagy and *(H)* ubiquitin proteasome pathway gene expression in cardiac tissue. $N = 5–7$ per group. All data are expressed as mean ± SEM. $^{*}P \leq 0.05$, $^{**}P \leq 0.01$, and $^{***}P \leq 0.001$. QA, quadriceps; RQ, relative quantity; TA, tibialis anterior.


DOI: 10.1002/jcsm.12745

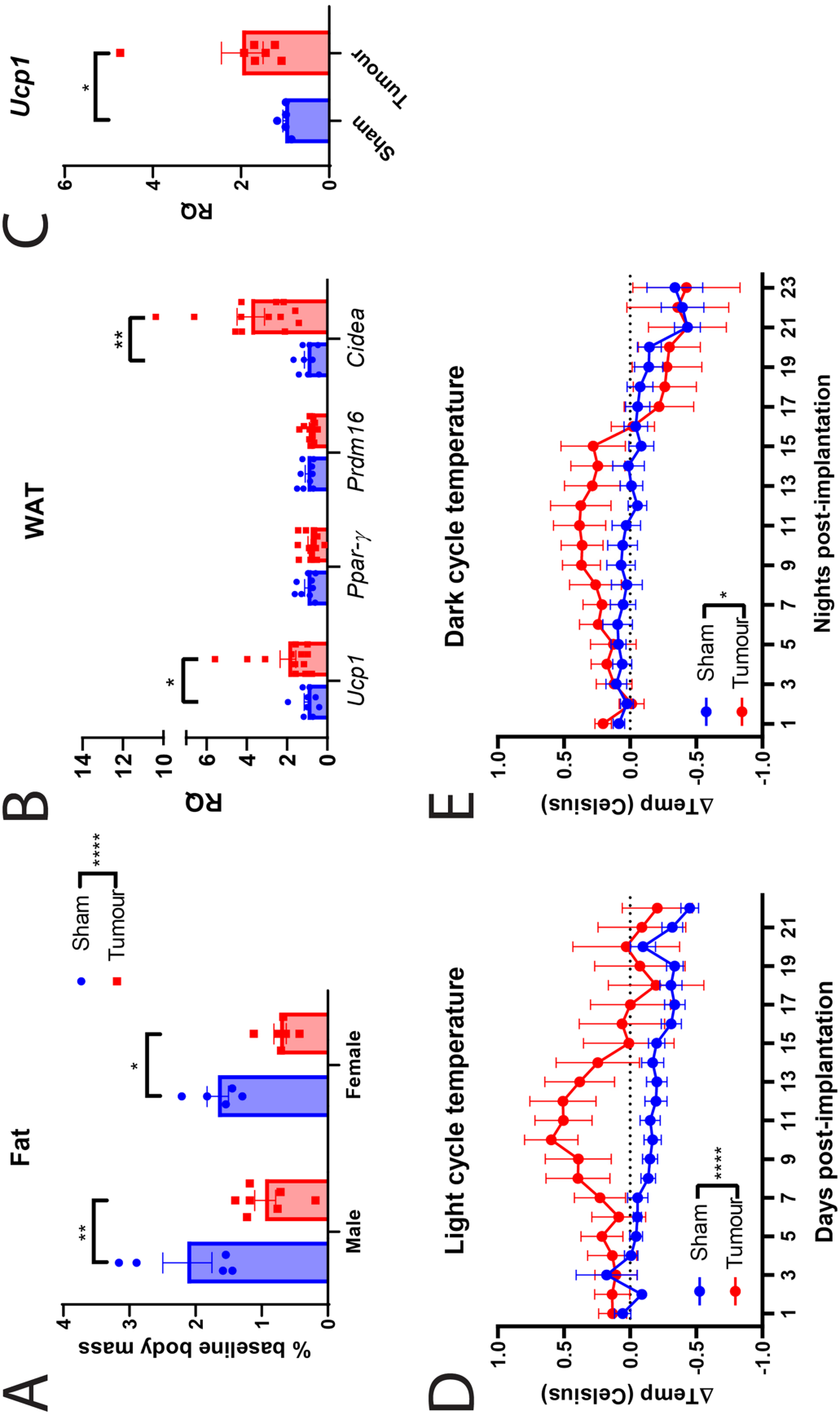


**Figure 5** MLM-cachexia results in white adipose tissue browning, elevation of thermogenesis in brown adipose tissue, and increased core body temperature. *(A)* Gonadal WAT mass normalized to body mass at the time of sacrifice. *(B)* WAT browning gene expression and *(C)* BAT *Ucp1* gene expression in male mice engrafted with MLM3 tumours or sham-operation controls. *(D)* Light and *(E)* dark cycle body temperature change in male mice engrafted with MLM tumours or sham-operation controls. *(A–C)* $N$ = 5–7 per group; *(B)* $N$ = 8–12 per group. *(D–E)* $N$ = 6 per group. All data are expressed as mean ± SEM. $^{*}P \leq 0.05$, $^{**}P \leq 0.01$, and $^{***}P \leq 0.001$. RQ, relative quantity; WAT, white adipose tissue.

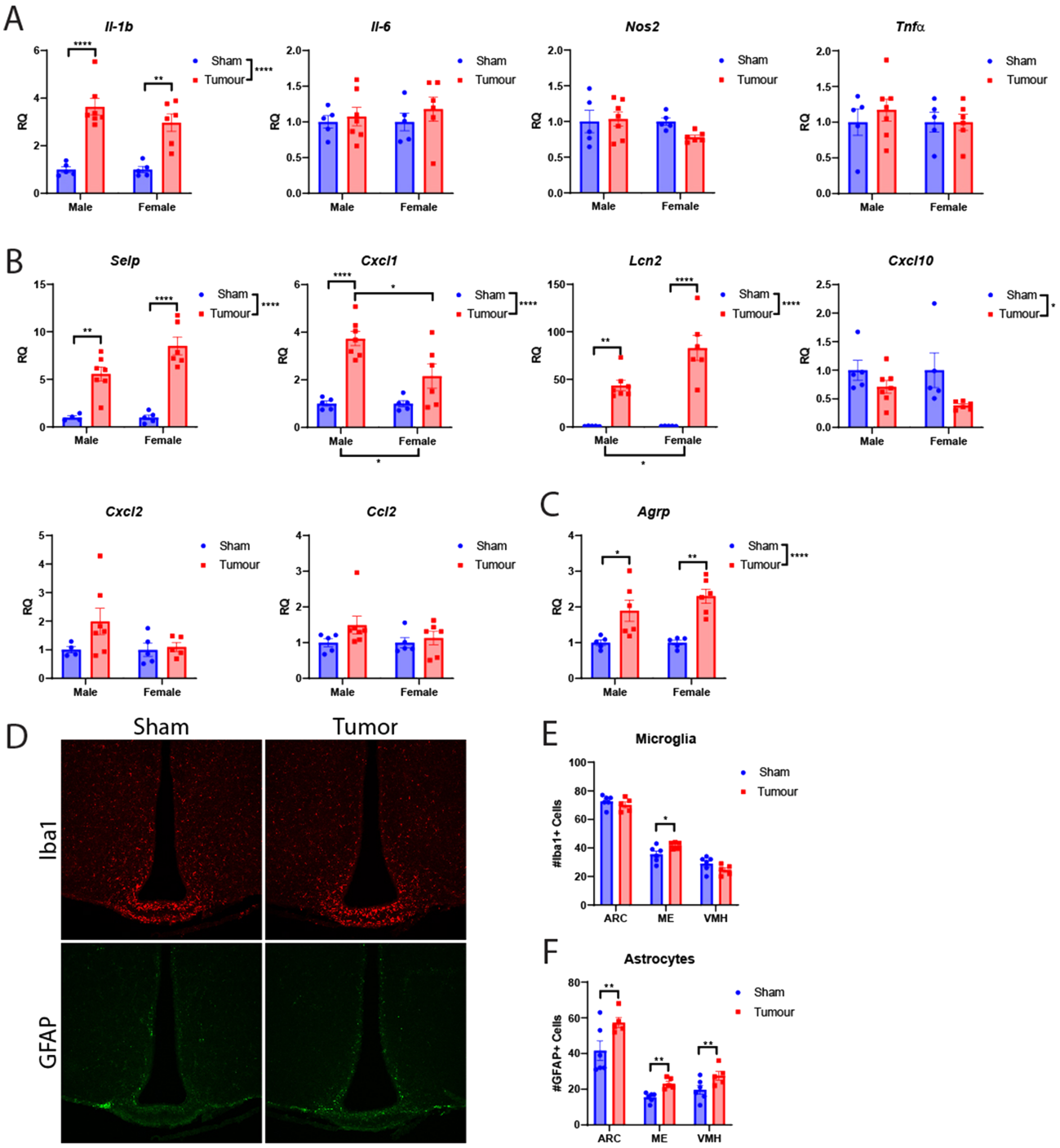


**Figure 6** MLM cachexia is associated with hypothalamic inflammation and gliosis in the mediobasal hypothalamus. *(A)* Hypothalamic inflammatory gene expression in MLM-engrafted and control mice. *(B)* Hypothalamic cell adhesion and chemokine-related genes in MLM-engrafted and control mice. *(C) Agrp* gene expression in MLM-engrafted and control mice. *(D)* Representative fluorescent immunohistochemistry images of the hypothalamus, staining for microglia (Iba1) and astrocytes (GFAP). (E) Microgliosis and *(F)* astrogliosis score in select hypothalamic regions in sham and tumour-bearing mice ($N$ = 6 per group). $N$ = 5–7 per group. All data are expressed as mean ± SEM. *$P \leq 0.05$, **$P \leq 0.01$, and ***$P \leq 0.001$. ARC, arcuate nucleus; ME, median eminence, RQ, relative quantity; VMH, ventromedial hypothalamus.

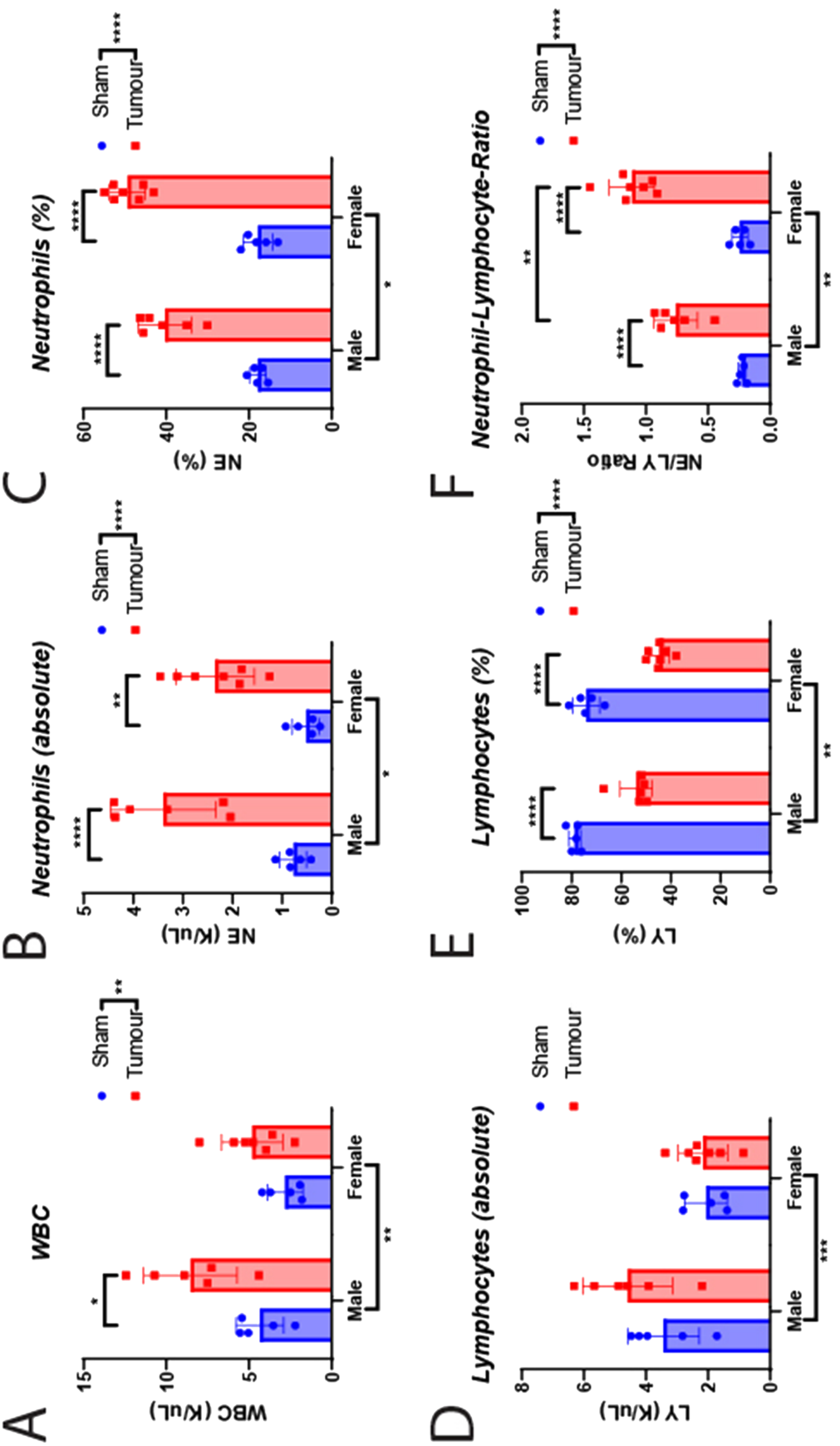


**Figure 7** MLM cachexia results in a neutrophil-dominant leukocytosis and an elevated neutrophil-to-lymphocyte ratio. *(A)* Absolute white blood cell, *(B)* neutrophil, and *(C)* lymphocyte levels in male and female mice engrafted with MLM3 tumours or sham-operation controls. *(D)* Relative neutrophil levels, *(E)* relative lymphocyte levels, and *(F)* neutrophil-to-lymphocyte ratios in male and female mice engrafted with MLM3 tumours or sham-operation controls. $N = 5–7$ per group. All data are expressed as mean ± SEM. $^{*}P \leq 0.05$, $^{**}P \leq 0.01$, and $^{***}P \leq 0.001$. LY, lymphocyte; NE, neutrophil; WBC, white blood cell.

count was elevated in tumour-bearing female mice, but not male mice (*Table* S1).

### *MLM3-cachexia results in systemic inflammation and alterations in hepatic metabolic gene expression*

Hepatic processes are extensively involved in disease associated with cachexia through their ability to regulate both inflammatory and metabolic programmes. Indeed, we observe a significant elevation of canonical inflammatory cytokines *Il-1β* and *Il-6* in MLM3-engrafted mice (*Figure* 8A). The acute-phase protein *Orm1*, a known mediator of inflammation and energy homeostasis through its actions on the leptin receptor, was also significantly elevated in MLM3-engrafted mice (*Figure* 8B).[44,45] In addition to hepatic inflammation, the spleens of MLM-engrafted mice were larger than sham controls at the end of the study (*Figure* 8C). In the liver, tumour-implanted mice exhibited increased expression of key glycolytic gene *Hk2*, enzyme *Pck1*, and lactate metabolism gene *Mct4* (*Figure* 8D). Despite an elevated in gluconeogenesis (GNG) enzyme *Pck1*, hepatic *G6pc* was unchanged between tumour-bearing and control mice (*Figure* 8E). Expression of lipid metabolism gene *Ppar-α* was also unaffected by the presence of MLM3 tumours (*Figure* 8F). In addition to these alterations in glucose handling genes in the liver, both male and female MLM3-engrafted mice displayed progressive hypoglycaemia during the development of cachexia (*Figure* 8G).

### *Voluntary wheel running mitigates lean and fat mass wasting in MLM3-engrafted mice*

The effect of voluntary wheel running was next explored in MLM3-engrafted mice to determine if aerobic exercise improves cachexia-related wasting, as is frequently reported in other murine cachexia models.[46,47] We observed a non-significant improvement in body mass loss in MLM3-engrafted mice with access to a wheel compared with those without (*Figure* 9A–9B). Similarly, wheel running non-significantly improved food consumption in MLM3-engrafted mice (*Figure* 9C). Interestingly, we assessed fat mass throughout the study and observed a significant sparing of baseline fat mass for tumour-bearing wheel mice compared with their no-wheel counterparts (*Figure* 9D–9E). To our knowledge, this is the first report of voluntary wheel running demonstrating a fat-sparing effect during cancer cachexia, as most investigations are focused on lean mass sparing. Although total lean mass trended towards improvement in tumour-bearing wheel mice, terminal gastrocnemius and cardiac tissue mass was significantly improved (*Figure* 9H–9I). This discrepancy could be explained by cancer-related organomegaly of tissues that encode as lean mass by NMR, including the liver and spleen, that is observed in both human and murine cancer progression.[31,48–50] On the molecular level, sparing of skeletal muscle in tumour-bearing wheel mice was associated with reduced ubiquitin ligase gene expression (*Figure* S4). Finally, because voluntary wheel running is noted to have anti-tumour properties in a murine melanoma model, we measured both tumour volume and terminal tumour mass to determine if the fat and muscle sparing phenotype is attributable to reduced disease burden.[51] In this study, access to a wheel did not significantly alter tumour growth, suggesting alternative mechanisms are responsible for fat and lean mass sparing in the wheel-running group (*Figure* 9J–9K).

## Discussion

Although several pre-clinical models of cachexia exist, all have limitations associated with their biological semblance of human disease. For instance, few rodent models of cancer cachexia include metastatic progression, even though cachexia in a clinical setting is almost always associated with metastatic and advanced-stage disease. Indeed, the ability of cancer cells to metastasize to host organs and alter physiologic and metabolic outputs is a compelling area of cachexia research, yet therapeutic development in a pre-clinical setting is almost always performed on localized, early-stage cancers (for review, refer to Biswas and Acharyya[22]). Therefore, the development of clinically relevant metastatic murine models of cachexia is a necessary step towards understanding cachexia in the context of advanced-stage disease. Utilizing a HPV + oropharyngeal squamous cell carcinoma cell line implanted in the flank of mice that MLM, we robustly characterize the physiologic and behavioural parameters associated with cancer cachexia (Figure 10).[23] It is estimated that nearly 60% of patients with cancer of the head and neck develop cachexia, and because pulmonary metastases are most frequently observed in squamous cell carcinoma of the head and neck, this model readily captures key oncologic features of clinically observed HNC cachexia.[2,52,53] We therefore sought to determine if the present model also accurately reflects the molecular and behavioural features of cancer cachexia observed in both clinical and pre-clinical settings.

The MLM3 cachexia model recapitulates several behavioural features of cachexia observed in other pre-clinical models, including reductions in home-cage locomotion and voluntary wheel running. Because tumour-associated fatigue is the most common symptom of cancer at the time of diagnosis and significantly contributes to reduced quality of life, functional disability, and is associated with disease recurrence reduced overall survival in certain cancers, cachexia

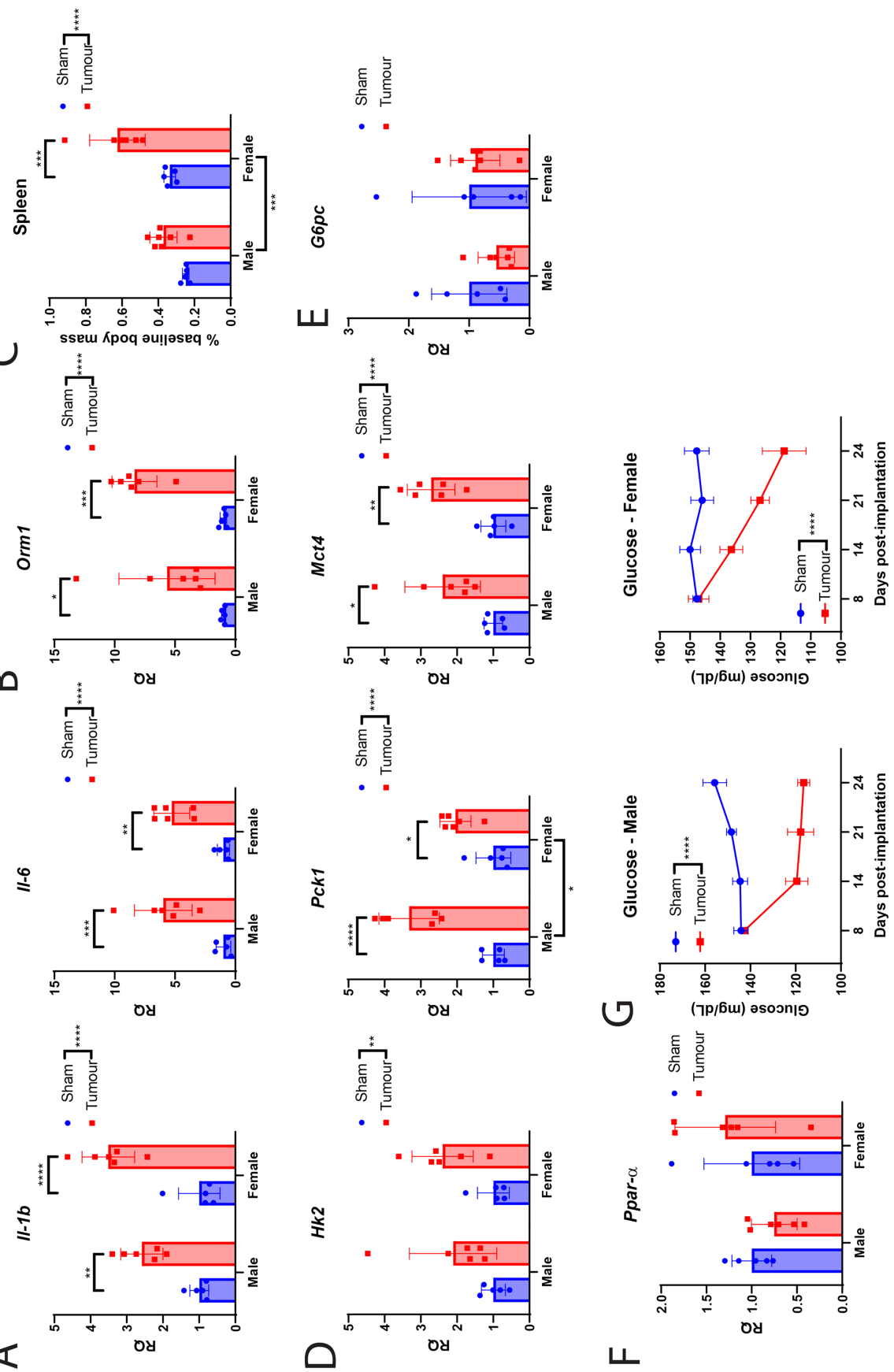


**Figure 8** MLM-cachexia results in hepatic and splenic inflammation and alteration in metabolic gene expression. *(A) Il-1β*, *Il-6*, and *(B) Orm1* hepatic gene expression in MLM3-engrafted and control mice. *(C)* Terminal spleen mass in MLM-engrafted and control mice. *(D)* Significantly regulated hepatic metabolic genes in MLM-engrafted and control mice. *(E) G6pc* and *(F) Ppar-α* gene expression in MLM-engrafted and control mice. *(G)* Repeated blood glucose measurements in male and female tumour-bearing and control mice. $N = 5–7$ per group. All data are expressed as mean ± SEM. $^{*}P \leq 0.05$, $^{**}P \leq 0.01$, and $^{***}P \leq 0.001$. RQ, relative quantity.

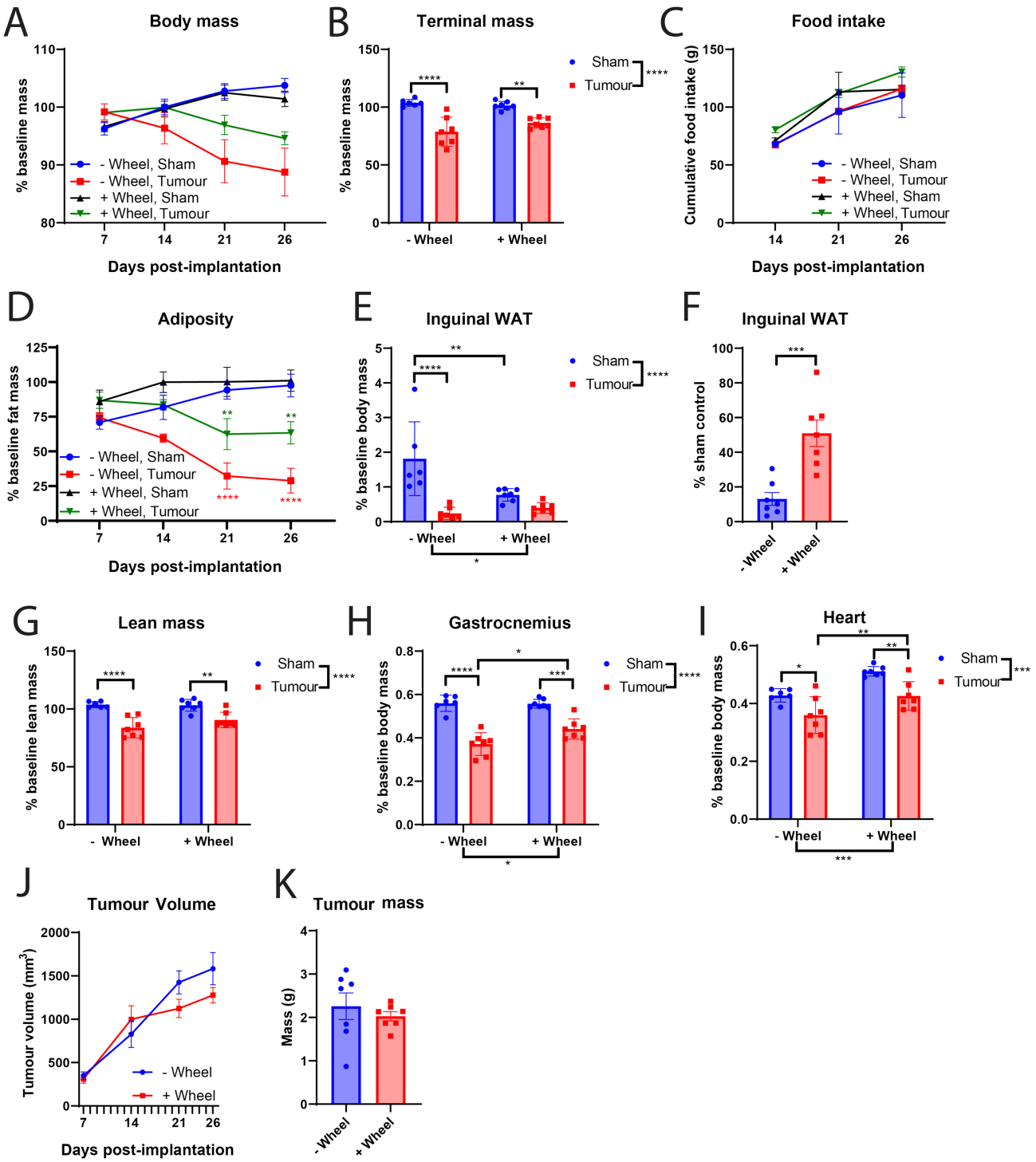


**Figure 9** Voluntary wheel running abrogates cachexia-associated fat and lean mass wasting in MLM3-engrafted mice. *(A)* Daily body mass, *(B)* tumour-free body mass, and *(C)* cumulative food intake in MLM3-engrafted and sham-operation controls with or without access to wheel running. *(D)* Sequential NMR fat mass, *(E)* terminal gonadal WAT mass, and *(F)* terminal sham-normalized WAT mass of MLM3-engrafted mice. *(G)* Terminal lean mass NMR, *(H)* gastrocnemius, and *(I)* cardiac tissue mass. *(J)* Tumour volume and *(K)* terminal tumour mass. $N$ = 6–7 per group. All data are expressed as mean ± SEM. $^{*}P \leq 0.05$, $^{**}P \leq 0.01$, and $^{***}P \leq 0.001$. WAT, white adipose tissue.

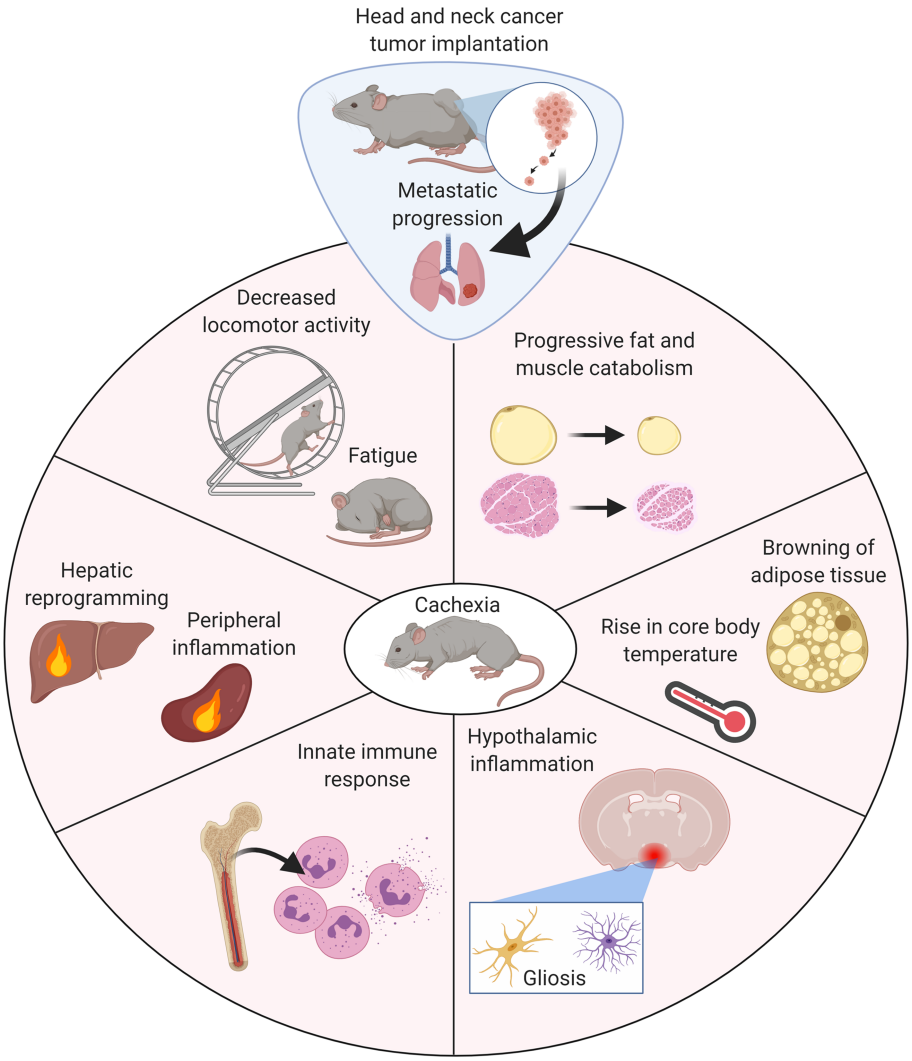


**Figure 10** Graphical summary of murine model head and neck cancer cachexia.

models should recapitulate this important behavioural response associated with cancer progression.[54–56] Indeed, the fatigue response associated with cancer cachexia is recapitulated in this MLM3 cancer cachexia model and mirrors that of human disease. Furthermore, we observe a significant lean-mass wasting phenotype that percolates to both fast-twitch and slow-twitch muscle groups, including the gastrocnemius, tibialis anterior, and quadriceps (fast-twitch), as well as the soleus (slow-twitch). The wasting of skeletal muscle in this model was associated with an elevated expression of E3 ubiquitin ligases *Murf1* and *Mafbx*, as well as their transcriptional regulator *Foxo1*. Importantly, while we report gene expression data for *Foxo1*, these data do not account for its activity level, which is regulated upon phosphorylation. Thus, these data are broadly associative but are in line with our NMR body composition analyses, as well as gross measurements, of muscle wasting in this model of cachexia. Cardiac tissue was modestly wasted in male mice, but not female mice, and was associated with an elevation in autophagy-related genes *Ctsl*, *Gabarapl*, and *Bnip3*. Interestingly, while other models of cancer cachexia report elevations in ubiquitin ligase genes in the heart, this axis of muscle wasting was not elevated in the MLM3 cachexia model in either male or female mice.[31] Several plausible explanations could explain the cardiac-sparing in MLM3-cachexia in female mice, including the role of improved nutrition in cardiac cachexia (as anorexia is absent in the MLM3 model), unique inflammatory cytokine profiles and signalling, involvement (or lack thereof) of the sympathetic nervous system on cardiac tissue, and specific tumour-derived factors' influence on cardiac pathophysiology.[28] Finally, because we observed a lower degree and number of MLM3-engrafted female mice experiencing metastatic lesions to the lung, it is possible that the metastatic cascade is critically important for the

development of wasting in this model. Additionally, female mice may experience lessened tissue catabolism due to their smaller tumour growth compared with their male counterparts. The decreased tumour growth and metastases may be explained, in part, by an immune mismatch of the implanted MLM cell line, as these clones were initially derived from a male mouse.[23] Finally, we characterize the effects of voluntary wheel running on cachexia-associated wasting and observe a significant sparing of lean mass in tumour-bearing animals that have access to a wheel, consistent with other models of cancer cachexia.[46,47]

Fat tissue physiology is increasingly recognized as a significant contributor the energy imbalance observed during cachexia. The importance of fat catabolism during cachexia is highlighted by the finding that WAT wasting frequently precedes that of muscle in patients suffering from cancer cachexia.[57] In addition to WAT, BAT serves to produce heat through thermogenesis, an evolutionarily conserved response that enables mammals to regulate their body temperature in cold environments. While lipid depletion, fibrosis, and immune cell invasion represent mechanisms contributing to fat tissue wasting and inflammation, 'browning' of white adipose, in which the expression of thermogenesis markers is elevated in WAT, remains a highly studied and debated topic of cachexia-related energy wasting.[41,58] Indeed, recent evidence for browning of WAT during cancer cachexia in humans and mice implores investigation into the contributions of fat to the pathogenesis of cachexia.[35,59] Interestingly, thermogenesis-related gene expression in WAT and BAT, such as cell death-inducing DFFA-like effector A and uncoupling protein 1, is inconsistently expressed among cachexia models. For instance, both C26 colonic adenocarcinoma and LLC allografts result in elevation of uncoupling protein 1 in WAT, while the KPC pancreatic ductal adenocarcinoma allograft results in decreased *Ucp1* expression.[31,35,60] These discrepancies in thermogenesis gene expression across cancer cachexia models remains unclear but could be partially explained by differences in nutritional status among these models, because caloric intake is a known mediator of adipose tissue browning.[61–63] With this in mind, we characterized browning signatures in male mice, as food consumption in the male tumour cohort was equivalent to that of sham controls, while female tumour-bearing mice exhibited significant hyperphagia near the end of our studies. We observed a significant elevation of browning markers *Ucp1* and *Cidea* in the WAT, with a concurrent increase in BAT *Ucp1*, in MLM3-engrafted male mice. Because tumour-derived PTHrP is a known mediator of adipose tissue browning in the LLC cachexia model, we assayed circulating levels of PTHrP in MLM-3 engrafted mice.[59] We observed no alteration of circulating PTHrP in the context of MLM3 cachexia, demonstrating the browning programmes induced by MLM3 progression is through alternative mechanisms. Furthermore, we observe a significant elevation of core body temperature in tumour-bearing mice compared with sham controls during middle stage disease, with a steady decline back to control animals towards end-stage disease. Although we observe increased thermogenesis gene expression in the BAT and WAT of MLM3-engrafted mice, along with a transient increase in core body temperature, these data are currently associative. Further mechanistic investigation is required to determine how (or if) browning of adipose tissue contributes to overall energy imbalance and cachexia progression in this model.

In addition to peripheral tissue catabolism and metabolic reprogramming, the CNS is a known mediator of metabolic dysfunction during cachexia. We and others described CNS-based mechanisms of cachexia in which systemic inflammatory signals are received and amplified by the hypothalamus, resulting in aberrant activity of weight-modulating and activity-modulating neurons.[4,28,64–67] To this end, we broadly characterized the inflammatory status in the mediobasal hypothalamus of MLM3-engrafted mice. We observed an elevation of the inflammatory cytokine *Il-1b* in cachectic mice after MLM3 implantation, along with an increase in hypothalamic glial cells (astrocytes and microglia). Indeed, an increase in hypothalamic *Il-1b* expression is also observed in other murine cachexia models, and hypothalamic expression of *Il-1b* in fenestrated capillaries is sufficient to induce illness behaviours consistent with cachexia symptoms in mice.[31,67–69] Despite clear evidence for the role of IL1 signalling in the regulation of illness behaviours, the precise role of IL1 signalling during cachexia remains elusive. For example, while IL1 signalling is elevated during cancer cachexia and is individually capable of inducing fatigue, tumour-associated fatigue develops independently of IL1 signalling, suggesting alternative inflammatory signals in the CNS drive fatigue symptoms during cachexia.[67,68] While microglia and astrocyte activation can be either pro-inflammatory or anti-inflammatory depending on the underlying condition, we recently reported the protective role of microglia in the hypothalamus in a murine model of pancreatic cancer cachexia.[37] Therefore, it remains to be determined if the gliosis observed in the present model is protective or detrimental. We also observe a significant elevation of hypothalamic cell adhesion and chemokine gene expression, including *Selp*, *Cxcl1*, and *Lcn2*. Recent works by Burfeind *et al*. demonstrate a clear role for myeloid cell invasion in the CNS in driving pancreatic cancer cachexia symptoms, including anorexia and lean mass catabolism, that is predominantly driven by the CCR2-CCL2 axis.[36] While we observe an elevation in several immune recruitment transcripts in the MLM3 cachexia model, we observe no difference in hypothalamic *Ccl2* expression. Given the unique immune recruitment gene expression profile we see in the hypothalami of MLM3-engrafted mice, whether or not immune cells invade the CNS, along with the specific role (if any) they serve in mediating cachexia symptoms, remain

an exciting area of future investigation. Finally, we observe an elevation of the orexigenic peptide *Agrp* in MLM3-engrafted mice, consistent with previous work describing an increase in *Agrp* gene expression in the context of chronic inflammation.[70] It is plausible that increased orexigenic peptide expression serves to prepare cachectic mice for a period of hyperphagia after inflammation subsides, ultimately in effort to replenish energy stores expended during the progression of cachexia.

From an immunologic perspective, the peripheral immune cell profile in the MLM3 model is consistent with that of cachectic patients. Decades of research describe an elevation in circulating neutrophils of patients with cancer, with an elevated NLR being associated with poorer survival outcomes both before and after treatment.[71,72] Indeed, an elevation in NLR is associated with weight loss and cachexia in patients with advanced colon, lung, and prostate cancer.[43] Despite the abundance of associative data concerning elevated NLR and patient outcomes, the influence of this immunologic shift during cachexia remains incompletely understood, ultimately highlighting the need for pre-clinical cachexia models that accurately reflect this immunologic shift for future mechanistic studies. Indeed, MLM3-engrafted mice display a neutrophil-dominant leukocytosis and elevated NLR, with tumour-bearing females exhibiting a significantly larger NLR than their male counterparts. This increased NLR in female mice may be explained by both baseline differences in neutrophil and lymphocyte counts, as well as some degree of neoantigenicity to the MLM3 clone, as this cell line was originally derived from a male mouse.[23] While it is generally appreciated that neutrophils play a vital role in the maintenance of lean muscle function through their interactions with tissue-resident macrophages, neutrophil invasion into muscle tissue after inflammatory challenge is associated with muscle membrane damage and reduced functionality.[73–75] With the drastic increase in circulating neutrophils in both cachectic patients and mice, it is plausible that this immunologic shift alters tissue physiology during cachexia, including muscle and fat catabolism and remodelling. Because the MLM3 cachexia model accurately reflects the circulating immune cell profile of human cachexia, we believe this model is well suited for future mechanistic studies concerning the role of the immune system during cancer cachexia.

Cancer cachexia is also associated with a shift in hepatic processes that increase the overall energy deficit through both futile cycling of metabolic intermediates and activation of the acute-phase response. It is well known that the lactate produced by tumour cell growth is reconverted to glucose in the liver via the Cori cycle. This axis is energetically demanding, as 6 ATP are consumed per glucose molecule produced, and it is hypothesized that these aberrant hepatic processes significantly contribute to the energy deficit incurred during the development of cachexia.[76] In addition to glucose produced by the Cori cycle, an elevation in hepatic GNG during tumour progression ultimately provides more glucose substrate for the growing tumour. However, because the MLM3-engrafted mice exhibit an increase in both hepatic gluconeogenic (*Pck1*) and glycolytic (*Hk2*) gene expression, it is unclear if hepatic processes contribute to the overall hypoglycaemia observed during tumour progression. It is plausible that an internal competition between muscle and the growing tumour for the depleting glucose stores drives some of the behavioural features of cachexia we observe in this model, including fatigue.[77] Notably, in contrast to our findings of increased GNG gene *Pck1*, Grossberg *et al*. observe a decrease in hepatic GNG genes in the parental non-metastatic cell line to MLM3, mEER, suggesting that MLM3 tumours differentially influence hepatic glucose handling from its parental cell line.[77] Indeed, the livers of MLM3-engrafted mice displayed an elevation in inflammation and acute-phase response genes, as well as an increase in gluconeogenic and lactate metabolism gene expression, consistent with hepatic processes observed in human cancer cachexia.[78–80]

While the MLM3 cachexia model recapitulates several key molecular and behavioural features of cancer cachexia, the model does have its limitations. Similar to other subcutaneous tumour models, positioning the tumour inoculum in an area in the flank that is not accessible to the mouse is imperative in preventing ulcerations and bleeding. Along these lines, the flank technically represents a heterotopic implantation site of the MLM3 cell line, as the parental cell line was generated from mouse tonsillar epithelium.[27,81] Although MLM3 implantation in the oropharynx may be possible to induce weight loss, it is likely that the wasting phenotype would be mostly attributable to the growth of the primary tumour directly in the aerodigestive tract and subsequent influence on caloric intake. However, subcutaneous engraftment of MLM3 cells still represents an epithelial implantation site and thus represents a more biologically relevant implantation site when compared with other commonly used subcutaneous allograft models, including LLC (lung adenocarcinoma) and C26 (colonic adenocarcinoma) to name a few. When implanted in the flank, this model of cachexia is not associated with anorexia, a cachexia symptom that is often observed in a clinical setting. However, while the absence of anorexia in this model may have its limitations, the nutrition-independent wasting phenotype observed has its advantages: (i) assessment of nutrition-influenced processes of cachexia, including adipose tissue thermogenesis, require technically challenging pair-feeding studies—this model circumvents the need for pair-feeding for accurate assessment of these parameters, and (ii) not all models of cachexia accurately assess the contributions of food intake on fat and muscle wasting—our characterization of the MLM3 model provides clear evidence that significant fat and muscle wasting occurs in the context

of adequate nutrition. To our knowledge, this is the first described syngeneic HNC cachexia model in C57BL/6 mice and the most widely used mouse strain with numerous genetically modified strains, ultimately enabling investigators wider access to knockout mouse variations for mechanistic studies. Finally, we also characterized an identically derived clone to MLM3, MLM5, with near-identical primary tumour growth.[23] Despite similar disease burden, MLM5-engrafted mice were significantly spared from cachexia-associated fat and lean mass wasting when compared with their MLM3-engrafted counterparts. However, MLM5 implantation was associated with an approximately 20% lower incidence of lung metastases, and this reduction in metastatic burden may explain some of the reduced cachexia features associated with this cell line. MLM5-engrafted mice also displayed a hyperphagic phenotype compared with both sham and MLM3-engrafted mice, which may also partly explain their improved cachexia status. Nevertheless, we believe that *in vivo* and *in vitro* comparisons of these two clones represent a unique resource for the identification of tumour-derived factors that may explain, in part, the cachexia-inducing potential of MLM3.

The MLM3 model described herein is simple, reliable, and recapitulates key features of cachexia observed in humans with metastatic HNC. It is generally assumed that the wasting associated with human HNC is predominantly due to tumour-related dysphagia. This model produces cachexia symptoms in the absence of dysphagia and anorexia, allowing for the investigation of nutrition-independent mechanisms of HNC cachexia. Although resistant to a standard chemoradiation (e.g. cisplatin), as is often the case in HNC patients with disease recurrence and progression, the MLM3 model provides a platform for the assessment of both anti-tumour and cachexia-inducing effects of experimental drugs for refractory HNC.[23] Given the large prevalence of cachexia in patients with HNC, yet development of very few pre-clinical models of metastatic and/or HNC cachexia, we believe this work helps bridge this gap in cachexia research. Collectively, our studies indicate that this metastatic HNC model accurately captures the signs and symptoms of clinically observed cachexia and provides the field a valuable tool for future mechanistic and therapeutic investigation.

## Acknowledgements

We thank Dr. Paola Vermeer of Sanford Research for kindly providing MLM cells derived in her laboratory. The graphical abstract was created using biorender (Biorender.com). The authors of this manuscript certify that they comply with the ethical guidelines for authorship and publishing in the *Journal of Cachexia, Sarcopenia and Muscle*.[82]

## Funding

This work was supported by NCI R01 CA184324 (Marks), the Brenden-Colson Center for Pancreatic Care (Marks), as well as NCI F30 CA254033 (Olson).

## Online supplementary material

Additional supporting information may be found online in the Supporting Information section at the end of the article.

**Figure S1.** Related to Figure 1. (A) Terminal tumor mass in MLM3 and MLM5 engrafted male mice. (B) Ubiquitin proteasome pathway gene expression in gastrocnemius muscle in sham, MLM3-, and MLM5-implanted mice. (C) Blood glucose levels in sham, MLM3-, and MLM5-implanted mice. (D) *Il-1b, Il-6, and Orm1* hepatic gene expression in sham, MLM3-, and MLM5-implanted mice. (E) Terminal splenic mass in in sham, MLM3-, and MLM5-implanted mice. RQ = relative quantity.

**Figure S2.** Related to Figure 2. (A) Tumor volume and terminal tumor mass in MLM3-engrafted male and female mice. (B-C) Representative H&E histochemical images of primary MLM3 tumors, highlighting areas of (B) ragged stromal infiltration and (C) focal necrotic loci. (D) Representative image of diseased lungs with metastatic lesions (arrows), and (E) representative histochemical image of microscopic metastatic MLM3 lesion (arrow).

**Figure S3.** Related to Figure 5. (A) Representative H&E histochemical images of gonadal white adipose tissue of male mice after sham operation or MLM3 tumor engraftment. (B) BAT *Ucp1* expression in male and female mice after sham operation or MLM3 tumor engraftment. Plasma PTHrP levels in (C) male and (D) female mice after sham operation or MLM3 tumor engraftment. (E) WAT browning gene expression in sham, MLM3-, and MLM5-engrafted mice. RQ = relative quantity. WAT = white adipose tissue.

**Figure S4.** Related to Figure 9. Ubiquitin proteasome pathway gene expression in gastrocnemius muscle in MLM3-engrafted and sham-operation controls with or without access to wheel running. RQ = relative quantity.

**Table S1.** Hematologic parameters of MLM3-implanted and sham-control mice. WBC = white blood cell. MCV = Mean corpuscular volume. MCH = mean corpuscular hemoglobin. MCHC = mean corpuscular hemoglobin concentration. RDW = Red Cell Distribution Width. MPV = Mean platelet volume. NE/LY = Neutrophil to lymphocyte ratio.

## Conflict of interest

DM is a consultant for Pfizer, Inc. and Alkermes, Inc. DM is a consultant, has received grant funding, and has equity in Tensive Controls, Inc. BO, MN, PL, and XZ declare that they have no conflict of interest.

## References


1. Grossberg AJ, Scarlett JM, Marks DL. Hypothalamic mechanisms in cachexia. *Physiol Behav* 2010;**100**:478–489.
2. Baracos VE, Martin L, Korc M, Guttridge DC, Fearon KCH. Cancer-associated cachexia. *Nat Rev Dis Primers* 2018;**4**:17105.
3. Tisdale MJ. Biology of cachexia. *J Natl Cancer Inst* 1997;**89**:1763–1773.
4. Olson B, Marks DL. Pretreatment cancer-related cognitive impairment-mechanisms and outlook. *Cancers (Basel)* 2019;**11**:687, https://doi.org/10.3390/cancers11050687
5. von Haehling S, Anker SD. Cachexia as a major underestimated and unmet medical need: facts and numbers. *J Cachexia Sarcopenia Muscle* 2010;**1**:1–5.
6. von Haehling S, Anker MS, Anker SD. Prevalence and clinical impact of cachexia in chronic illness in Europe, USA, and Japan: facts and numbers update 2016. *J Cachexia Sarcopenia Muscle* 2016;**7**:507–509.
7. Mueller TC, Bachmann J, Prokopchuk O, Friess H, Martignoni ME. Molecular pathways leading to loss of skeletal muscle mass in cancer cachexia—can findings from animal models be translated to humans? *BMC Cancer* 2016;**16**:75.
8. Morley JE, von Haehling S, Anker SD. Are we closer to having drugs to treat muscle wasting disease? *J Cachexia Sarcopenia Muscle* 2014;**5**:83–87.
9. Le-Rademacher JG, Crawford J, Evans WJ, Jatoi A. Overcoming obstacles in the design of cancer anorexia/weight loss trials. *Crit Rev Oncol Hematol* 2017;**117**:30–37.
10. Baracos VE. Clinical trials of cancer cachexia therapy, now and hereafter. *J Clin Oncol* 2013;**31**:1257–1258.
11. Penna F, Busquets S, Argilés JM. Experimental cancer cachexia: evolving strategies for getting closer to the human scenario. *Semin Cell Dev Biol* 2016;**54**:20–27.
12. Tomasin R, Martin A, Cominetti MR. Metastasis and cachexia: alongside in clinics, but not so in animal models. *J Cachexia Sarcopenia Muscle* 2019;**10**:1183–1194.
13. Konishi M, Ebner N, von Haehling S, Anker SD, Springer J. Developing models for cachexia and their implications in drug discovery. *Expert Opin Drug Discovery* 2015;**10**:743–752.
14. Bennani-Baiti N, Walsh D. Animal models of the cancer anorexia-cachexia syndrome. *Support Care Cancer* 2011;**19**:1451–1463.
15. Argilés JM, Busquets S, Stemmler B, López-Soriano FJ. Cancer cachexia: understanding the molecular basis. *Nat Rev Cancer* 2014;**14**:754–762.
16. Vanhoutte G, van de Wiel M, Wouters K, Sels M, Bartolomeeussen L, De Keersmaecker S, et al. Cachexia in cancer: what is in the definition? *BMJ Open Gastroenterol* 2016;**3**:e000097, https://doi.org/10.1136/bmjgast-2016-000097
17. Loberg RD, Bradley DA, Tomlins SA, Chinnaiyan AM, Pienta KJ. The lethal phenotype of cancer: the molecular basis of death due to malignancy. *CA Cancer J Clin* 2007;**57**:225–241.
18. Consul N, Guo X, Coker C, Lopez-Pintado S, Hibshoosh H, Zhao B, et al. Monitoring metastasis and cachexia in a patient with breast cancer: a case study. *Clin Med Insights Oncol* 2016;**10**:83–94.
19. Shiono M, Huang K, Downey RJ, Consul N, Villanueva N, Beck K, et al. An analysis of the relationship between metastases and cachexia in lung cancer patients. *Cancer Med* 2016;**5**:2641–2648.
20. Waning DL, Mohammad KS, Reiken S, Xie W, Andersson DC, John S, et al. Excess TGF-β mediates muscle weakness associated with bone metastases in mice. *Nat Med* 2015;**21**:1262–1271.
21. Wang G, Biswas AK, Ma W, Kandpal M, Coker C, Grandgenett PM, et al. Metastatic cancers promote cachexia through ZIP14 upregulation in skeletal muscle. *Nat Med* 2018;**24**:770–781.
22. Biswas AK, Acharyya S. Understanding cachexia in the context of metastatic progression. *Nat Rev Cancer* 2020;**20**:274–284.
23. Vermeer DW, Coppock JD, Zeng E, Lee KM, Spanos WC, Onken MD, et al. Metastatic model of HPV+ oropharyngeal squamous cell carcinoma demonstrates heterogeneity in tumor metastasis. *Oncotarget* 2016;**7**:24194–24207.
24. Olson B, Edwards J, Stone L, Jiang A, Zhu X, Holland J, et al. Association of sarcopenia with oncologic outcomes of primary surgery or definitive radiotherapy among patients with localized oropharyngeal squamous cell carcinoma. *JAMA Otolaryngol Head Neck Surg* 2020;**146**:1–9.
25. Jager-Wittenaar H, Dijkstra PU, Dijkstra G, Dijkstra G, Bijzet J, Langendijk JA, et al. High prevalence of cachexia in newly diagnosed head and neck cancer patients: an exploratory study. *Nutrition (Burbank, Los Angeles County, Calif)* 2017;**35**:114–118.
26. Anker MS, Holcomb R, Muscaritoli M, von Haehling S, Haverkamp W, Jatoi A, et al. Orphan disease status of cancer cachexia in the USA and in the European Union: a systematic review. *J Cachexia Sarcopenia Muscle* 2019;**10**:22–34.
27. Hoover AC, Spanos WC, Harris GF, Anderson ME, Klingelhutz AJ, Lee JH. The role of human papillomavirus 16 E6 in anchorage-independent and invasive growth of mouse tonsil epithelium. *Arch Otolaryngol--Head Neck Surgery* 2007;**133**:495–502.
28. Olson B, Zhu X, Norgard MA, Levasseur PR, Butler JT, Buenafe A, et al. Lipocalin 2 mediates appetite suppression during pancreatic cancer cachexia. *Nat Commun* 2021;**12**:2057.
29. Deacon RM. Assessing nest building in mice. *Nat Protoc* 2006;**1**:1117–1119.
30. Meijer JH, Robbers Y. Wheel running in the wild. *Proc Biol Sci* 2014;**281**:20140210, https://doi.org/10.1098/rspb.2014.0210
31. Michaelis KA, Zhu X, Burfeind KG, Krasnow SM, Levasseur PR, Morgan TK, et al. Establishment and characterization of a novel murine model of pancreatic cancer cachexia. *J Cachexia Sarcopenia Muscle* 2017;**8**:824–838.
32. Cai D, Frantz JD, Tawa NE Jr, OhBC L. IKKbeta/NF-kappaB activation causes severe muscle wasting in mice. *Cell* 2004;**119**:285–298.
33. Zhang G, Jin B, Li YP. C/EBPβ mediates tumour-induced ubiquitin ligase atrogin1/MAFbx upregulation and muscle wasting. *EMBO J* 2011;**30**:4323–4335.
34. Acharyya S, Ladner KJ, Nelsen LL, Damrauer J, Reiser PJ, Swoap S, et al. Cancer cachexia is regulated by selective targeting of skeletal muscle gene products. *J Clin Invest* 2004;**114**:370–378.
35. Petruzzelli M, Schweiger M, Schreiber R, Campos-Olivas R, Tsoli M, Allen J, et al. A switch from white to brown fat increases energy expenditure in cancer-associated cachexia. *Cell Metab* 2014;**20**:433–447.
36. Burfeind KG, Zhu X, Norgard MA, Levasseur PR, Huisman C, Buenafe AC, et al. Circulating myeloid cells invade the central nervous system to mediate cachexia during pancreatic cancer. *Elife* 2020;**9**:e54095, https://doi.org/10.7554/eLife.54095
37. Burfeind KG, Zhu X, Norgard MA, Levasseur PR, Huisman C, Michaelis KA, et al. Microglia in the hypothalamus respond to tumor-derived factors and are protective against cachexia during pancreatic cancer. *Glia* 2020;**68**:1479–1494.
38. Olson B, Marks DL, Grossberg AJ. Diverging metabolic programmes and behaviours during states of starvation, protein malnutrition, and cachexia. *J Cachexia Sarcopenia Muscle* 2020;**11**:1429–1446.
39. Lee S, Kim JH, Kim JH, Seo JW, Han HS, Lee WH, et al. Lipocalin-2 is a chemokine inducer in the central nervous system: role of chemokine ligand 10 (CXCL10) in lipocalin-2-induced cell migration. *J Biol Chem* 2011;**286**:43855–43870.
40. Schroll A, Eller K, Feistritzer C, Nairz M, Sonnw eber T, Moser PA, et al. Lipocalin-2 ameliorates granulocyte functionality. *Eur J Immunol* 2012;**42**:3346–3357.
41. Baazim H, Schweiger M, Moschinger M, Xu H, Scherer T, Popa A, et al. CD8(+) T cells induce cachexia during chronic viral infection. *Nat Immunol* 2019;**20**:701–710.
42. Xu C, Yuan J, Du W, Wu J, Fang Q, Zhang X, et al. Significance of the neutrophil-to-lymphocyte ratio in p16-negative squamous cell carcinoma of unknown primary in head and neck. *Front Oncol* 2020;**10**:39.
43. Barker T, Fulde G, Moulton B, Nadauld LD, Rhodes T. An elevated neutrophil-to-lymphocyte ratio associates with weight loss and cachexia in cancer. *Sci Rep* 2020;**10**:7535–7535.
44. Sun Y, Yang Y, Qin Z, Cai J, Guo X, Tang Y, et al. The acute-phase protein orosomucoid regulates food intake and

energy homeostasis via leptin receptor signaling pathway. *Diabetes* 2016;**65**: 1630–1641.
45. Lee YS, Choi JW, Hwang I, Lee JW, Lee JH, Kim AY, et al. Adipocytokine orosomucoid integrates inflammatory and metabolic signals to preserve energy homeostasis by resolving immoderate inflammation. *J Biol Chem* 2010;**285**:22174–22185.
46. Pigna E, Berardi E, Aulino P, Rizzuto E, Zampieri S, Carraro U, et al. Aerobic exercise and pharmacological treatments counteract cachexia by modulating autophagy in colon cancer. *Sci Rep* 2016;**6**:26991, https://doi.org/10.1038/srep26991
47. Khamoui AV, Park BS, Kim DH, Yeh MC, Oh SL, Elam ML, et al. Aerobic and resistance training dependent skeletal muscle plasticity in the colon-26 murine model of cancer cachexia. *Metabolism: Clin Experiment* 2016;**65**:685–698.
48. Lieffers JR, Mourtzakis M, Hall KD, McCargar LJ, Prado CM, Baracos VE. A viscerally driven cachexia syndrome in patients with advanced colorectal cancer: contributions of organ and tumor mass to whole-body energy demands. *Am J Clin Nutr* 2009;**89**:1173–1179.
49. Bonetto A, Rupert JE, Barreto R, Zimmers TA. The colon-26 carcinoma tumor-bearing mouse as a model for the study of cancer cachexia. *J Vis Exp: JoVE* 2016;https://doi.org/10.3791/54893
50. Hojo H, Enya S, Arai M, Suzuki Y, Nojiri T, Kangawa K, et al. Remote reprogramming of hepatic circadian transcriptome by breast cancer. *Oncotarget* 2017;**8**: 34128–34140.
51. Pedersen L, Idorn M, Olofsson GH, Lauenborg B, Nookaew I, Hansen RH, et al. Voluntary running suppresses tumor growth through epinephrine- and IL-6-dependent NK cell mobilization and redistribution. *Cell Metab* 2016;**23**:554–562.
52. Ferlito A, Shaha AR, Silver CE, Rinaldo A, Mondin V. Incidence and sites of distant metastases from head and neck cancer. *ORL J Otorhinolaryngol Relat Spec* 2001;**63**:202–207.
53. Stone L, Olson B, Mowery A, Krasnow S, Jiang A, Li R, et al. Association between sarcopenia and mortality in patients undergoing surgical excision of head and neck cancer. *JAMA Otolaryngol Head Neck Surg* 2019;**145**:647–654.
54. Visser MR, van Lanschot JJ, van der Velden J, Kloek JJ, Gouma DJ, Sprangers MA. Quality of life in newly diagnosed cancer patients waiting for surgery is seriously impaired. *J Surg Oncol* 2006;**93**:571–577.
55. Brown DJ, McMillan DC, Milroy R. The correlation between fatigue, physical function, the systemic inflammatory response, and psychological distress in patients with advanced lung cancer. *Cancer* 2005;**103**: 377–382.
56. Groenvold M, Petersen MA, Idler E, Bjorner JB, Fayers PM, Mouridsen HT. Psychological distress and fatigue predicted recurrence and survival in primary breast cancer patients. *Breast Cancer Res Treat* 2007;**105**:209–219.
57. Fouladiun M, Körner U, Bosaeus I, Daneryd P, Hyltander A, Lundholm KG. Body composition and time course changes in regional distribution of fat and lean tissue in unselected cancer patients on palliative care—correlations with food intake, metabolism, exercise capacity, and hormones. *Cancer* 2005;**103**:2189–2198.
58. Batista ML Jr, Henriques FS, Neves RX, Olivan MR, Matos-Neto EM, Alcântara PS, et al. Cachexia-associated adipose tissue morphological rearrangement in gastrointestinal cancer patients. *J Cachexia Sarcopenia Muscle* 2016;**7**:37–47.
59. Kir S, White JP, Kleiner S, Kazak L, Cohen P, Baracos VE, et al. Tumour-derived PTH-related protein triggers adipose tissue browning and cancer cachexia. *Nature* 2014;**513**:100–104.
60. Rohm M, Schäfer M, Laurent V, Üstünel BE, Niopek K, Algire C, et al. An AMP-activated protein kinase-stabilizing peptide ameliorates adipose tissue wasting in cancer cachexia in mice. *Nat Med* 2016;**22**: 1120–1130.
61. Kim KH, Kim YH, Son JE, Lee JH, Kim S, Choe MS, et al. Intermittent fasting promotes adipose thermogenesis and metabolic homeostasis via VEGF-mediated alternative activation of macrophage. *Cell Res* 2017;**27**:1309–1326.
62. Li G, Xie C, Lu S, Nichols RG, Tian Y, Li L, et al. Intermittent fasting promotes white adipose browning and decreases obesity by shaping the gut microbiota. *Cell Metab* 2017;**26**:801.
63. Rothwell NJ, Stock MJ. A role for brown adipose tissue in diet-induced thermogenesis. *Obes Res* 1997;**5**:650–656.
64. Burfeind KG, Michaelis KA, Marks DL. The central role of hypothalamic inflammation in the acute illness response and cachexia. *Semin Cell Dev Biol* 2016;**54**: 42–52.
65. Braun TP, Zhu X, Szumowski M, Scott GD, Grossberg AJ, Levasseur PR, et al. Central nervous system inflammation induces muscle atrophy via activation of the hypothalamic-pituitary-adrenal axis. *J Exp Med* 2011;**208**:2449–2463.
66. Grossberg AJ, Zhu X, Leinninger GM, Levasseur PR, Braun TP, Myers MG, et al. Inflammation-induced lethargy is mediated by suppression of orexin neuron activity. *J Neurosci* 2011;**31**:11376–11386.
67. Knoll JG, Krasnow SM, Marks DL. Interleukin-1β signaling in fenestrated capillaries is sufficient to trigger sickness responses in mice. *J Neuroinflammation* 2017;**14**: 219.
68. Grossberg AJ, Vichaya EG, Christian DL, Molkentine JM, Vermeer DW, Gross PS, et al. Tumor-associated fatigue in cancer patients develops independently of IL1 signaling. *Cancer Res* 2018;**78**:695–705.
69. Liu X, Nemeth DP, McKim DB, Zhu L, DiSabato DJ, Berdysz O, et al. Cell-type-specific interleukin 1 receptor 1 signaling in the brain regulates distinct neuroimmune activities. *Immunity* 2019; **50**:317–333, e6.
70. Scarlett JM, Zhu X, Enriori PJ, Bowe DD, Batra AK, Levasseur PR, et al. Regulation of agouti-related protein messenger ribonucleic acid transcription and peptide secretion by acute and chronic inflammation. *Endocrinology* 2008;**149**:4837–4845.
71. Howard R, Kanetsky PA, Egan KM. Exploring the prognostic value of the neutrophil-to-lymphocyte ratio in cancer. *Sci Rep* 2019;**9**:19673, https://doi.org/10.1038/s41598-019-56218-z
72. Viñal D, Gutierrez-Sainz L, Martinez D, Garcia-Cuesta JA, Pedregosa J, Villamayor J, et al. Prognostic value of neutrophil-to-lymphocyte ratio in advanced cancer patients receiving immunotherapy. *Clin Transl Oncol* 2021;**23**:1185–1192. https://doi.org/10.1007/s12094-020-02509-1
73. Frenette J, St-Pierre M, Côté CH, Mylona E, Pizza FX. Muscle impairment occurs rapidly and precedes inflammatory cell accumulation after mechanical loading. *Am J Physiol Regul Integr Comp Physiol* 2002;**282**: R351–R357.
74. Tidball JG. Regulation of muscle growth and regeneration by the immune system. *Nat Rev Immunol* 2017;**17**:165–178.
75. Dumont N, Bouchard P, Frenette J. Neutrophil-induced skeletal muscle damage: a calculated and controlled response following hindlimb unloading and reloading. *Am J Physiol Regul Integr Comp Physiol* 2008; **295**:R1831–R1838.
76. Friesen DE, Baracos VE, Tuszynski JA. Modeling the energetic cost of cancer as a result of altered energy metabolism: implications for cachexia. *Theor Biol Med Model* 2015;**12**:17.
77. Grossberg AJ, Vichaya EG, Gross PS, Ford BG, Scott KA, Estrada D, et al. Interleukin 6-independent metabolic reprogramming as a driver of cancer-related fatigue. *Brain Behav Immun* 2020;**88**: 230–241.
78. Holroyde CP, Skutches CL, Boden G, Reichard GA. Glucose metabolism in cachectic patients with colorectal cancer. *Cancer Res* 1984;**44**:5910–5913.
79. Tisdale MJ. Mechanisms of cancer cachexia. *Physiol Rev* 2009;**89**:381–410.
80. Holroyde CP, Gabuzda TG, Putnam RC, Paul P, Reichard GA. Altered glucose metabolism in metastatic carcinoma. *Cancer Res* 1975;**35**:3710–3714.
81. Spanos WC, Hoover A, Harris GF, Wu S, Strand GL, Anderson ME, et al. The PDZ binding motif of human papillomavirus type 16 E6 induces PTPN13 loss, which allows anchorage-independent growth and synergizes with ras for invasive growth. *J Virol* 2008;**82**:2493–2500.
82. von Haehling S, Morley JE, Coats AJS, Anker SD. Ethical guidelines for publishing in the Journal of Cachexia, Sarcopenia and Muscle: update 2019. *J Cachexia Sarcopenia Muscle* 2019;**10**:1143–1145.